High dynamic shift behaviour of automated manual transmissions in sportscar application

Masterthesis

by

Timofej Kuchtar

Adviser

Assoc.Prof. Dipl.-Ing. Dr.techn. Mario Hirz

Technical University Graz

Faculty Mechanical Engineering and Economic Sciences

Institute of Automotive Engineering

Univ.-Prof. Dipl.-Ing. Dr.techn. Peter Fischer

Graz, September 2017

STATUTORY DECLARATION

I declare that I have authored this thesis independently, that I have not used other than the declared sources / resources, and that I have explicitly marked all material which has been quoted either literally or by content from the used sources.

Graz, …… ……

(signature)

Abstract

This thesis describes how predefined circumstances are created to investigate high dynamic shift behaviour on an automated manual transmission (AMT). The modelling of a look up table engine with realistic torsional vibrations and torque delays is shown. A detailed multiplate clutch model considering rotational and axial friction and therefore unequal force and torque distribution is built. The automated manual transmission is implemented as an existing sFunction from LMS Amesim (Siemens Product Lifecycle Management Software Inc.). All models are then combined and connected to a simple longitudinal vehicle model. This vehicle model is then used to simulate power-on upshifts which are then evaluated.

Table of contents

1 List of symbols

a	[-]	Parameter 1 for combustion torque approximation
a_{boost}	[-]	Boost ratio
b	[-]	Parameter 2 for combustion torque approximation
$c_{onepack}$	[N/m]	Substitutional stiffness for one clutch plate pair
c_{pc}	[J/kgK]	Specific heat capacity compressor intake
c_{pt}	[J/kgK]	Specific heat capacity turbine gas
c_t	[-]	Orifice discharge coefficient
d	[-]	Function offset
d_{fpad}	[Ns/m]	Friction plad damping rate
$d_{fpcplate}$	[Ns/m]	Friction plad carrier plate damping rate
d_{fplate}	[Ns/m]	Friction plate damping rate
$d_{onepack}$	[Ns/m]	Substitutional damping rate for one clutch plate pair
$g(v)$	[m]	LuGre function for friction calculation
h_a	[J/kg]	Exhaust gas specific enthalpy
$h_{c,adi}$	[J/kg]	Intake gas specific enthalpy
h_e	[J/kg]	Intake gas specific enthalpy
k	[-]	Scaling factor
m	[kg]	Mass
m_a	[kg]	Exhaust gas mass
$\dot{m}_{at}$	[kg/s]	Mass flow past throttle plate
$\dot{m}_{at,0}$	[kg/s]	Fitting constant
$\dot{m}_c$	[kg/s]	Compressor mass flow
$\dot{m}_{c,cor}$	[kg/s]	Corrected compressor mass flow
m_{cr}	[kg]	Oscillating part of conrod mass
m_e	[kg]	Intake gas mass
m_f	[kg]	Fuel mass
$\dot{m}_f$	[kg/s]	Fuel mass flow
$\dot{m}_{ff}$	[kg/s]	Fuel film mass flow
$\dot{m}_{fi}$	[kg/s]	Fuel film mass flow into cylinder

m_{fplate}	[kg]	Friction plate mass
$\dot{m}_{fv}$	[kg/s]	Fuel vapour mass flow
m_{leak}	[kg]	Combustion leakage mass
m_{pist}	[kg]	Piston mass including piston pin
$\dot{m}_t$	[kg/s]	Turbine mass flow
m_{vibe}	[-]	Form factor for vibe function
n	[-]	Polytropic factor
n_{eng}	[n/min]	Engine speed
$n_{tc,cor}$	[n/min]	Corrected turbocharger speed
p	[bar]	Cylinder pressure
p_{amb}	[bar]	Ambient pressure
$p_{cyl,0}$	[bar]	Intake pressure
$p_{cyl,lp}(\varphi)$	[bar]	Cylinder pressure low pressure cycle
p_{man}	[bar]	Intake manifold pressure
p_{me}	[bar]	Mean effective cylinder pressure
p_{mi}	[bar]	Mean indicated cylinder pressure
p_{mr}	[bar]	Mean friction pressure
p_r	[-]	Pressure ratio
p_1	[bar]	Pressure at compressor inlet
p_2	[bar]	Pressure at compressor outlet
p_3	[bar]	Pressure at turbine inlet
p_4	[bar]	Pressure at turbine outlet
r_{cs}	[m]	Crankshaft throw radius
s_i	[-]	Speed sample
s_{pist}	[m]	Piston position
s_{tot}	[-]	Total amount of speed samples
t	[s]	Time
t_{fpad}	[mm]	Friction plad thickness
$t_{fpcplate}$	[mm]	Friction plad carrier plate thickness
t_{fplate}	[mm]	Friction plate thickness
t_{tot}	[s]	Total time the combustion lasts
v_d	[m/s]	LuGre dynamic damping parameter
v	[m/s]	Velocity between friction surfaces

v_s	[m/s]	LuGre Stribeck velocity parameter
w	[m/s]	Characteristic speed
x_a	[-]	Output signal for the PT1 element
x_{br}	[-]	Burn rate
x_e	[-]	Input signal for the PT1 element
$x_{fpcplate}$	[m]	Friction pad carrier plate position
$\dot{x}_{fpcplate}$	[m/s]	Friction pad carrier plate velocity
x_{fplate}	[m]	Friction plate position
$\dot{x}_{fplate}$	[m/s]	Friction plate velocity
$\ddot{x}_{fplate}$	[m/s^2]	Friction plate acceleration
y	[-]	Function output
z	[m]	Average bristle deformation
A_{bore}	[mm^2]	Cylinder bore area
A_{fpad}	[mm^2]	Friction plad area
$A_{fpcplate}$	[mm^2]	Friction plad carrier plate area
A_{fplate}	[mm^2]	Friction plate area
A_t	[mm^2]	Throttle plate area
C	[-]	Constant
C_1	[-]	Constant
D_v	[m/s]	Velocity intervall
E_{fpad}	[N/mm^2]	Friction plad young modulus
$E_{fpcplate}$	[N/mm^2]	Friction plad carrier plate young modulus
E_{fplate}	[N/mm^2]	Friction plate young modulus
$F_D(v)$	[N]	Dynamic friction force
F_N	[N]	Normal force on friction surface
F_R	[N]	Friction force
F_{Ri}	[N]	Friction force acting on friction plate
F_{ext}	[N]	External force
$F_{g,lp}(\varphi)$	[N]	Gas force low pressure cycle
F_{in}	[N]	Input force acting on friction plate
F_m	[N]	Mass intertia force
F_{out}	[N]	Output force acting on friction plate

F_{pist}	[N]	Force on the piston
F_r	[N]	LuGre resulting friction force
F_t	[N]	Force on the crankpin
F_v	[N]	LuGre viscous friction force
H_u	[J/kg]	Lower heating value
I	[kgm^2]	Inertia
I_{eng}	[kgm^2]	Engine intertia
I_{load}	[kgm^2]	Intertia of the load
J_{tc}	[kgm^2]	Turbocharger inertia
M_{basic}	[Nm]	Basic torque without combustion
M_c	[Nm]	Compressor torque
M_{eng}	[Nm]	Resulting engine torque
$M_{eng,i}$	[Nm]	Indicated engine torque
M_f	[Nm]	Turbocharger friction torque
$M_{g,comb}$	[Nm]	Resulting torque at crankshaft
$M_{g,lp}$	[Nm]	Low pressure engine cycle torque
M_m	[Nm]	Torque due to oscillating masses
M_{pist}	[Nm]	Torque at crankshaft due to piston force
M_r	[Nm]	Engine friction torque
M_t	[Nm]	Turbine torque
M_{tc}	[Nm]	Turbocharger theoretically available torque
$M_{tc,del}$	[Nm]	Turbocharger delayed torque
P_b	[W]	Load
P_c	[W]	Compressor power
P_f	[W]	Friction power
P_p	[W]	Pump losses
$P_{t,adi}$	[W]	Turbine power
R	[J/molK]	Ideal gas constant
T	[K]	Temperature
T_{amb}	[K]	Ambient temperature
T_{const}	[s]	Time constant PT1 element
T_{man}	[K]	Intake manifold temperature
T_{tc}	[s]	Turbocharger torque delay time constant

T_1^*	[K]	Compressor inlet temperature
T_2^*	[K]	Compressor outlet temperature
T_3^*	[K]	Turbine inlet temperature
U	[J]	Internal energy
Q_B	[J]	Fuel energy release
Q_{Btot}	[J]	Net fuel energy released
Q_W	[J]	Wall heat transfer energy
V	[mm³]	Volume
$V_{cyl,0}$	[mm³]	Cylinder volume at BDC
$V_{cyl,\varphi}$	[mm³]	Cylinder volume
V_d	[mm³]	Engine displacement
V_{man}	[mm³]	Intake manifold volume
X	[-]	Fuel film fraction
$\eta_{c,is}$	[-]	Isentropic compressor efficiency
η_i	[-]	Thermal efficiency
η_m	[-]	Mechanical efficiency
$\eta_{t,is}$	[-]	Isentropic turbine efficiency
η_{vol}	[-]	Volumetric efficiency
λ_{cr}	[-]	Ratio of Stroke to connecting rod length
α	[rad]	Throttle angle
α_G	[W/m²K]	Heat transfer coefficient
α_0	[rad]	Throttle angle at idle
$\beta_1(\alpha)$	[-]	Effective throttle area function
$\beta_2(p_{man})$	[-]	Outflow function
κ	[-]	Heat capacity ratio
κ_c	[-]	Heat capacity ratio compressor intake
κ_c	[-]	Heat capacity ratio turbine gas
μ	[-]	Friction coefficient
μ_S	[-]	Static friction coefficient
ρ_0	[kg/m³]	Density before compressor
ρ_1	[kg/m³]	Density after compressor
σ_0	[N/m]	Bristle stiffness
$\sigma_1(v)$	[m/s]	Bristle dynamic damping ratio

τ_d	[s]	Time delay engine dynamics
τ_{ff}	[s]	Time constant fuel vaporisation
φ	[°cs]	Crankshaft angle
ω_{tc}	[rad/s]	Turbocharger angular velocity

2 Introduction

This thesis was created in collaboration with hofer forschungs- und entwicklungs GmbH.

Automated manual transmissions are conquering two sectors in the automotive industry, small car and sportscar applications. The advantage for small cars being the simplicity of an ordinary manual transmission, therefore lower costs but with the partial comfort of an automatic transmission. Partial comfort because while on the one hand the usability is the same as for an automatic transmission, giving the advantage in traffic of not having to operate the clutch and manually shift gears, on the other hand the driving comfort is lower due to the necessary interruption of torque in order to be able to shift gears. This comfort disadvantage is not present in dualclutch transmissions and is the reason for them being used in middle class car applications and partially in sportscar applications, where they fit in even with a higher cost factor. As mentioned before, AMTs became a strong competitor to the dual clutch transmissions (DCTs) in sportscar applications, because there is a limit for the two clutches in transmittable torque, size and therefore inertia. Unlike a DCT, an AMT can be built with every clutch type available and is due to just one smaller clutch and less rotating parts with in total less inertia and overall weight much more suitable for a car where vehicle dynamics are key factors. The disadvantage of the torque interruption vanishes because in sportscar applications a small jerk is not a statement of a low standard shifting process but sometimes even wanted for a sporty and crisp feeling that gives the impression of shorter shift times.

The process to develop a powertrain is very complex. Size, material and stiffness are influencing the design and controller development. With the introduction of computer aided support over time, recourses were shifted to the early stage of development of a product. Using digital and virtual models, a significant part of the design process is covered. The process called frontloading became very important. In this thesis it is shown how different models are built to simulate an entire powertrain using MATLAB Simulink (The MathWorks, Inc., 2015).

Power-on upshifts are investigated after building the models. To get as much insight into a shift as possible, the engine model includes oscillating mass torque, compression and ignition torque pulses on the crankshaft. The clutch model contains a rotational and axial friction model to be able to simulate unequal clutchplate force distribution on a multiplate clutch. A detailed transmission and driveshaft model is implemented from an existing LMS Amesim model present as an sFunction to sum up the simple longitudinal vehicle model. Using this longitudinal vehicle model two types of upshifts are simulated and discussed.

3 Task definietion

As described before, a significant part of the development of a car is done by the use of computer aided engineering. Early virtual testing will support the decisions during development. With the development of a new hybrid sportscar the demand for simulations in various development areas is created. The powertrain architecture is a hybrid P1 layout with a 6 cylinder turbocharged gasoline engine. Additional to an electric motor that is connected to the crankshaft, another one, connected to the turbocharger, is used. A dry multiplate clutch connects the automated manual transmission to the engine. One topic of interest is how the components of the powertrain will function together and how the gearbox can perform to achieve the best shift performance and shift behaviour. Therefore a simplified longitudinal model needs to be created. To investigate how engine torque oscillations affect the drivetrain, an engine model is demanded, that can provide these oscillations. Furthermore a clutch model has to be created, that can depict the axial force loss due to the multiplate layout. An existing model of the automated manual transmission needs to be parametrised to match the manufacturer synchronization times. Engine, clutch and transmission models then need to be coupled and implemented into a simplified longitudinal model. Using the complete model it has to be shown, that shift behaviour investigations can be performed. This needs to be done by simulation and discussion of upshifts. The tasks can now be clearly defined as:

- Create engine model with torsional oscillations
- Create dry multiplate clutch model with axial force loss
- Implement models of the engine, clutch and Transmission into simplified longitudinal model
- Parametrize automated manual transmission to match synchronization times estimated by the manufacturer
- Simulate and discuss upshifts to show model functionality

The following chapters will provide a theoretical insight needed to fulfil the tasks and a solution for each point is presented.

4 Theoretical

Computer aided engineering is very important in today's development of almost every product. It is used in many different areas to accelerate the engineering process. This can be a digital mock up model to check the fitment of all parts, three dimensional design where the shape is used further in one department to verify its rigidity and stiffness using finite elements calculations and in another its aerodynamic qualities using continuous fluid dynamics software, or virtual systems that represent real parts describing them with mathematical relationships. This gives a huge area of application, not only in frontloading, but also in research. Virtual systems can be built to replicate reality or better understand the behaviour of real systems and have many other areas of application, for example data can be extracted from areas no sensor could be placed because of space, or because it would affect the result too much due to its mass or thermal inertia. There are several software products that allow building virtual models using logic and mathematical operation blocks. One of them is MATLAB Simulink. In the software environment it is possible to perform textual and graphical programming and with its own language to work with matrices and arrays. MATLAB Simulink's flexibility makes it attractive to be applied in a wide field of application, one area being engineering. The longitudinal model in this thesis is built within this software product. The model has a modular setup, which is oriented to the main parts of a powertrain. The following chapters explain possible modelling of these submodels and the mechanics behind them.

4.1 Powertrain

A powertrain is an assembly of components that propel a car, which includes torque and speed generation and their transformation. The torque generation can be performed through a combustion engine, an electric motor or a combination of both, then called a hybrid powerunit. Connecting shafts and one or more clutches are responsible for the torque transfer. To transform torque, mainly gears are used, packaged into a cluster and a casing, called the gearbox. A basic powertrain is shown in **Figure 1**.

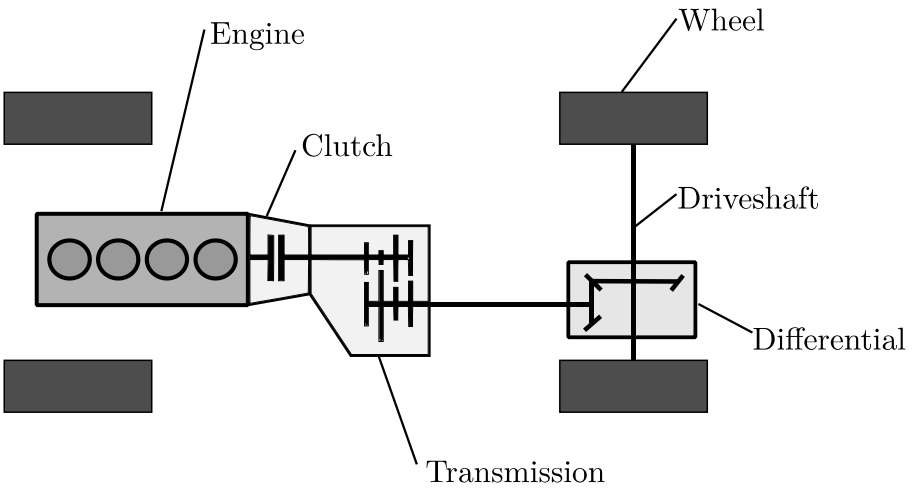

Figure 1: Conventional powertrain layout

This layout can be described with a combustion engine delivering the torque, which is interrupted or transferred to a gearbox by the clutch. After the torque transformation inside of the gearbox, a torque split in a differential takes place. Following the differential the distributed torque reaches the wheelhubs, rims and tires via driveshafts. Seeking better fuel economy and lower exhaust gas emissions is a driving factor of intensive development. Besides complicated and innovative engine design and management, electrification is one important step to reach the goals. Hybrid powertrains vary in where the electric motor is placed, how powerful it is and its control strategy. Each layout has its drawbacks and benefits. For example, the motor can be placed after the clutch between gearbox and combustion engine, and allows to drive the car fully electric if the clutch is disengaged. **Figure 2** shows the layout of the described hybrid powertrain.

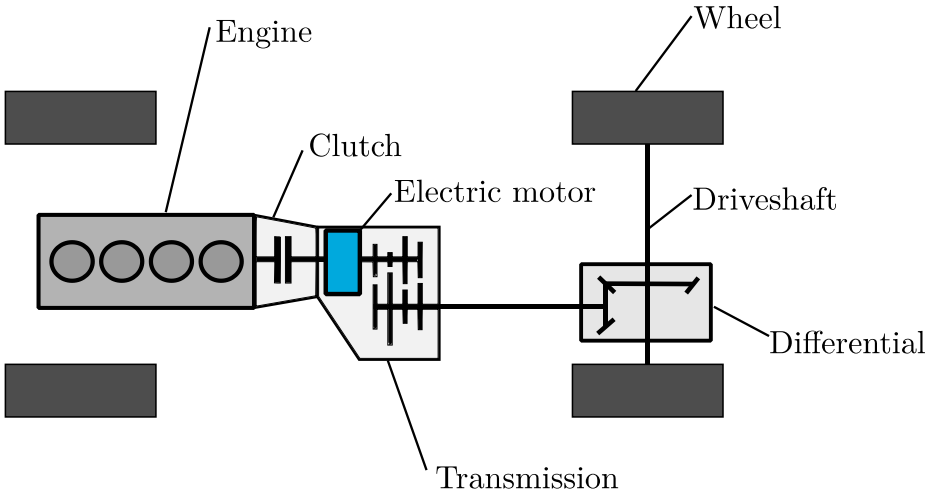

Figure 2: Hybrid powertrain with one electric motor between clutch and transmission known as P2 configuration

Another layout can be interesting for the entire vehicle dynamics. Two electric motors drive the two rear wheels allowing for torque vectoring implementation. This would allow to control the available torque separately between the left and right tire. Using this principle to have more torque on the outside tires of a turning car would result in a greater momentum over the cars vertical axis and thereby raise the vehicles dynamic abilities. In this instance the combustion engine drives only the front wheels as shown in **Figure 3**.

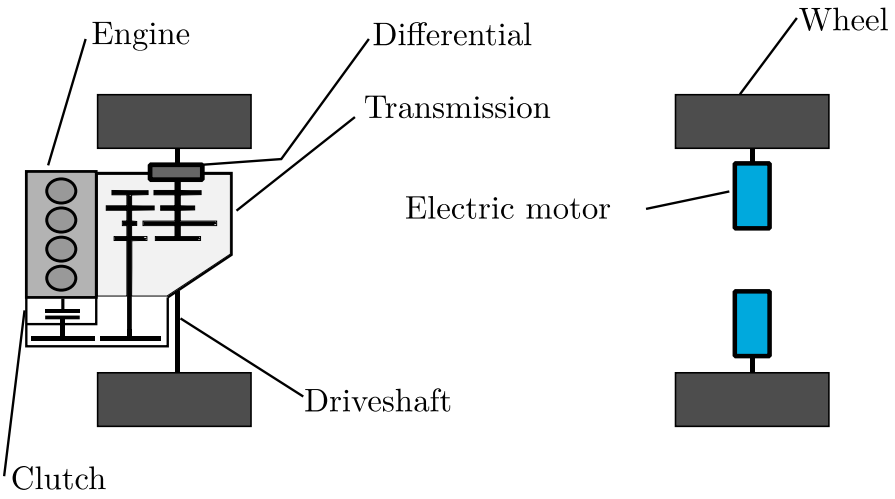

Figure 3: Hybrid powertrain with two electric motors on th rear axle, describing a P4 configuration

Another possibility is to attach an electric motor directly to the crankshaft and improve the dynamic behaviour of the combustion engine. This hybrid layout describes a P1 configuration. One of the benefits of hybrid powertrains and therefore a strategy to save fuel is the possibility to return energy back into the battery, or other storage systems. The electric motor can therefore operate as a generator to recuperate kinetic energy. The energy which would be transformed into heat by conventional brakes, can now be fed back into the system to a certain amount and again reused. While the battery development is ongoing and is essential for full electric vehicles, the hybrid system can already reduce the emissions of the current combustion engine powered vehicles and help with the development of electric components and their implementation.

4.2 Transmission

One of the key components in the powertrain is the transmission. Over time a variety of transmissions were developed depending on their field of use. They can be divided into four main types.

- Manual transmission
- Semi-automatic transmission
- Fully automatic transmission
- Mechanical continuously variable transmission

While the manual, semi-automatic, and fully automatic design use gears as torque transformation and thereby have fixed ratios to choose from, a mechanical continuously variable transmission (CVT) is designed to vary the ratio continuously. As an excerpt main types for passenger vehicles are explained.

4.2.1 Manual transmission

Manual transmissions represent a conventional type gearbox, consisting of constant meshed helical cut gears and synchronizers. Constant meshed means the input and output gears are always in contact. This design demands one gear to be fixed to its shaft and the other one to spin freely, when another pair of gears is engaged. In neutral, none of the idler gears is connected to its shaft. The free spinning gear is called idler gear. To transmit torque, the free spinning gear is

connected to its shaft by a teethed sleeve that establishes a connection between shaft, synchronizer body and the idler gear. The transmission is manually operated, this means to change gear the driver needs to operate a mechanical linkage that is connected to the synchronizers (Lechner & Naunheimer 1999, p.130). A general layout of such a manual transmission is shown in **Figure 4**. The gearwheels have different numbers of teeth and therefore different gear ratios which transform the torque and speed of the inputshaft to the outputshaft.

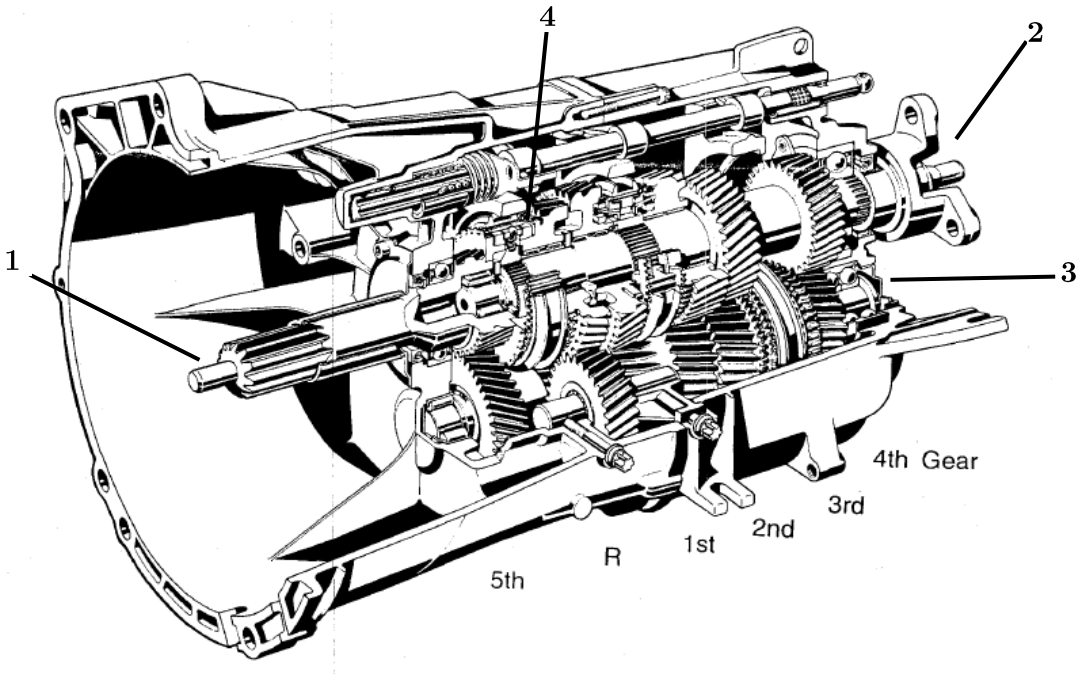

Figure 4: Manual transmission, with 1) inputshaft, 2) outputshaft, 3) countershaft, 4) crossection of synchronization unit (Lechner & Naunheimer 1999, p.316)

Therefore, shifting from one gear to another demands an adjustment of shaft speed and the synchronizers are designed to do that. A single cone synchronizer is shown in **Figure 5**. When the gear engagement process begins, a shiftfork moves the synchronizer sleeve towards the gear. With the detent mechanism built into the sleeve a conical synchronizer ring is also moved towards the synchronizer hub. The synchronizer hub is connected to the idler gear and therefore has a speed difference to the synchronizer ring and the sleeve. When the synchronizer ring has contact with the hub, a friction force emerges. This friction force slows down or accelerates the idler gear with the hub. While this synchronization

process takes place, the friction torque holds the synchronizer ring radially in place and positions its teeth against the teeth of the sleeve. This prevents further axial movement of the sleeve. As soon as the differential speed is eliminated, the torque acting on the synchronizer ring vanishes. With no torque acting on the synchronizer ring, its tapered teeth allow the sleeve to adjust the rings radial position and move past it. After passing the teeth of the ring, the sleeve engages with the splines of the synchronizer hub. By this the speeds are synchronized and a fixed connection between gear and shaft is created to transmit the torque. The losses in a manual transmission are lower than in a traditional automatic transmission (Lechner & Naunheimer 1999, p.55). In combination with a manual transmission, in most cases a single plate clutch is used.

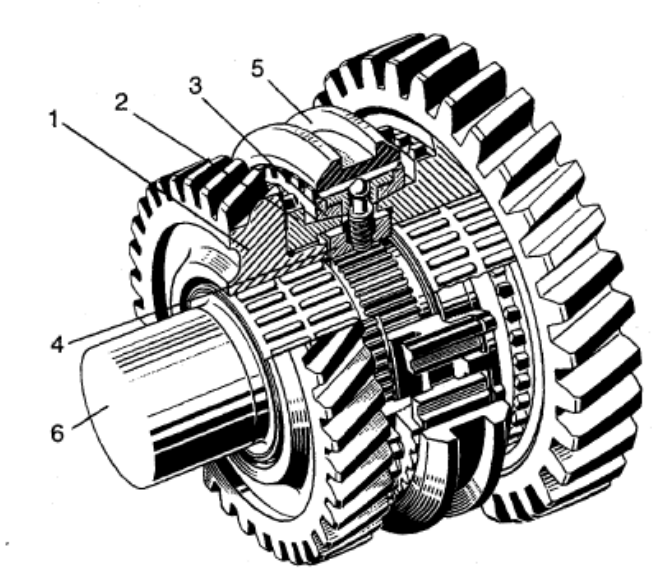

Figure 5: Synchronizer setup, with 1) idler gear, 2) synchronizer hub, 3) synchronizer ring, 4) synchronizer body, 5) synchronizer sleeve, 6) transmission shaft (Lechner & Naunheimer 1999, p.316)

4.2.2 Automatic transmission

4.2.2.1 Conventional automatic transmission

As a more comfortable type of gearbox with an intelligent and adaptive control system, this transmission performs the shifts automatically. In comparison to the manual transmission, the automatic gearbox is equipped with epicyclic gears and

instead of a clutch it uses a torque converter. The use of a torque converter in combination with the planetary gear setup allows shifting without power interruption. Not using synchronizers but clutch packs and brakes to shift gears is another difference to the manual gearbox (Lechner & Naunheimer 1999, p.135).

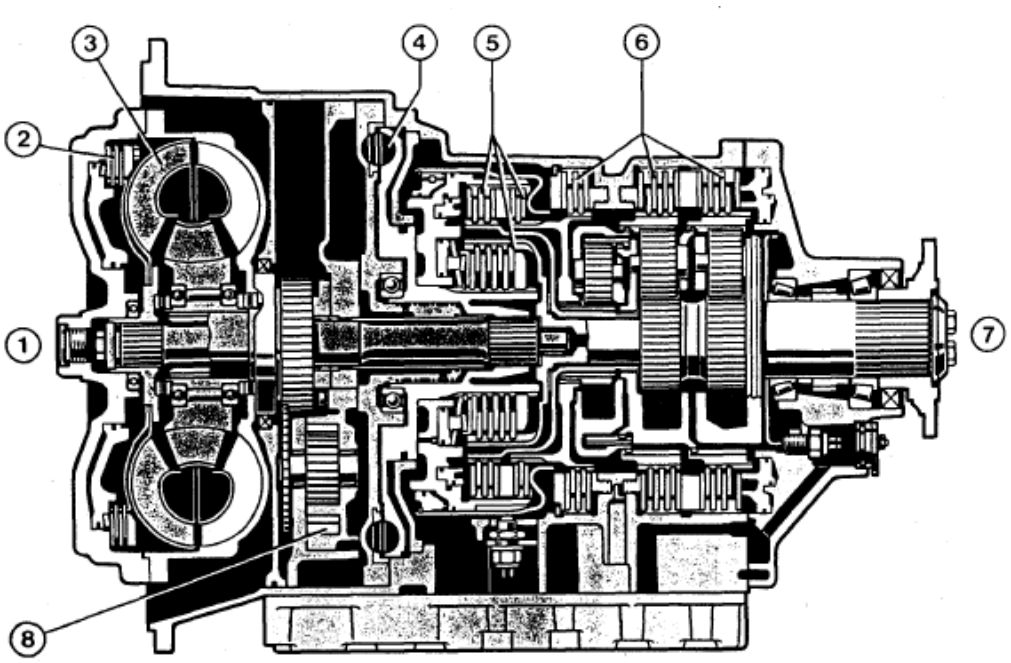

Figure 6: Automatic transmission with 1) input, 2) torque converter lockup-clutch, 3) torque converter 4) retarder, 5) clutches, 6) brakes, 7) output (Lechner & Naunheimer 1999, p.332)

The shift comfort is a result of the torque converters ability to convert speed and torque. The converter itself is acting thereby as a hydrodynamic transmission by using the fluid flow inertia in a closed flow circuit. A hydraulic pump, turbine and a reactor are positioned in one housing to allow a load dependent continuously variable ratio change. Due to the hydraulic conversion, there are losses through impact, friction, flow resistance and leakage (Lechner & Naunheimer 1999, p.261). These losses are quite significant and therefore a locking mechanism is used when the converter should have zero slip. By this design the overall efficiency of the transmission can be raised.

4.2.2.2 Automated manual transmissions

Another type of automatic transmissions is an automated manual transmission. This gearbox has the same components as a manual transmission, but the actuation of the clutch and gearchange mechanism is performed by actuators instead of the driver. These can be pure electric, electro hydraulic or electro pneumatic systems. With a current as input, the actuators output the desired force. Thereby shifts can be performed in an automated controlled manner. Due to the simple components used from a conventional manual transmission design, these gearboxes are finding their way into lower price segment cars and offer a good comfort and affordable automatic shifting. But this is not the only benefit. In comparison to the design space, and therefore transmittable torque limited dualclutch transmissions, an AMT can incorporate any type of clutch technology. For example, a multiplate clutch is smaller in its diameter compared to a singleplate clutch and saves rotational inertia, which is beneficial for the powertrain dynamics. The inertia is even lower due to the fact that a double clutch transmission needs two of them. With fully automated shift control, fast gear changes can be achieved. This opens the way for another automotive sector, the sportscars.

4.3 Engine model

Modelling a combustion engine can be done in different ways, but over time three main groups have been developed. The separation is based on the accuracy of their delivered results and their area of application. The following chapters provide a small overview over those three modelling possibilities and their purpose.

4.3.1 Look up table model

The simplest way to represent engine characteristics is a torque generator unit with a lookup table. Therefore, a specific torque number is put out depending on a two dimensional map using engine speed and throttleangle. An overall mass inertia combines all of the engines internals to one figure and makes it possible to

simulate engines dynamics. This approach provides fast calculation times and can be trimmed with different methods to behave similar to the real engine in defined test cases. Some of the improvements consist of delays and other ways to model torque build up. However, it will not be able to represent all scenarios in transient behaviour, and will not provide information on medium properties such as temperatures or pressures. The look up table model is the most common used model for gearbox control development and is satisfactory for this purpose.

4.3.2 Mean value engine model

To gain a deeper insight into detail what is happening during power generation the mean value engine model was introduced. It describes the engine based on thermodynamic and physical rules and can give information about generated temperatures and pressures. It uses energy and mass conservation equations across the engine to calculate missing variables (Theotokatos 2009, p.107). Hendricks and Sorenson (1990) state that this model calculates mean values over one or more engine cycles and uses instantaneous and time developing relations between variables. Instantaneous relationships are described by algebraic equations and reach equilibrium within one or a few engine cycles. Time developing relationships become differential or state equations and take 10 to 1000 engine cycles to reach equilibrium. As an example the time developing relations can be described through three state equations that can be determined from the laws of mass and energy conservation. (Hendricks and Sorenson 1990, p.1882-1883). Jyh-Shin Chen (2008) states that the model can be built up component wise where the connections represent actual physical connections. This makes it possible to reuse already modelled objects. For example choosing massflow, pressure and enthalpy as variables transmitted and received across the ports of the submodels, will define the state of one substance entirely and can be used further in the submodels equations (Jyh-Shin Chen 2008, p.3). The mean value engine model is capable to predict different variables, which are important for engine and its peripheral development at a resolution not higher than one or more cycles. Therefore this model is not able to depict in cycle variations. When the initial conditions for one cycle are the same as for the previous one, fixed

thermodynamic boundary conditions do not allow for cycle by cycle variations like random combustion pressure variations in spark ignited engines (Guzzella and Onder 2004, p.22). One possible modelling approach is described by the following relationships for the state equations. The state variables are represented by the air manifold pressure, fuel mass flow and the crankshaft speed. The differential equation for the manifold pressure

$$\dot{p}_{man} = -\frac{n_{eng}\, V_d}{120\, V_{man}}\, \eta_{vol}\, p_{man} + \frac{R\, T_{man}}{V_{man}}\, \dot{m}_{at}(\alpha, p_{man}) \tag{1}$$

is shown in (1). Where V_d is the engine displacement, V_{man}, T_{man} and p_{man} the manifold volume, temperature and pressure. Engine speed is represented through n_{Eng} (Hendricks and Sorenson 1990, p.1883). The volumetric efficiency η_{vol} accounts for the losses during an intake stroke and is therefore the ratio between the air to fuel mixture entering the cylinder in comparison to the air to fuel mixture that would occupy the cylinder under the conditions present in the intake manifold. R defines the ideal gas constant. The mass flow past the throttle plate is described by

$$\dot{m}_{at}(\alpha, p_{man}) = c_t\, A_t\, \frac{p_{amb}\, \sqrt{\kappa'}}{\sqrt{R\, T_{amb}}}\, \beta_1(\alpha)\, \beta_2(p_{man}) + \dot{m}_{at0} \tag{2}$$

and can be modelled as the flow of a compressible medium through a converging nozzle. A_t describes the effective area of the nozzle and T_{amb} and p_{amb} the ambient temperature and pressure. A fitting constant is defined by $\dot{m}_{at0}$. With κ being the isentropic heat capacity ratio

$$\kappa' = \frac{2\,\kappa}{\kappa - 1} \tag{3}$$

can be defined. The function

$$\beta_1(\alpha) = 1 - \cos(\alpha - \alpha_0) \tag{4}$$

represents the dependency on the throttle valve opening angle α relative to its idle opening position α_0. The function

$$\beta_2(p_{man}) = \begin{cases} \sqrt{p_r^{\frac{2}{\kappa}} - p_r^{\frac{\kappa+\kappa}{\kappa}}} & ,if\ p_r \geq \left(\frac{2}{\kappa+1}\right)^{\frac{\kappa}{\kappa-1}} \\ \sqrt{\left(\frac{1}{\kappa'}\right)\left(\frac{2}{\kappa+1}\right)^{\frac{\kappa+1}{\kappa-1}}} & ,otherwise \end{cases} \quad (5)$$

models the behaviour for two flow cases, the subsonic and the sonic air flow. The pressure ratio between p_{man} and p_{amb} is defined by p_r (Hendricks and Sorenson 1990, p.1884). C_t is a coefficient that describes the frictional losses through the throttle valve (Chaing, Zhu, and Patankar 2007, p.126). Hendricks and Sorenson (1990) describe a simple model that divides the fuel mass entering the cylinder

$$\dot{m}_f = \dot{m}_{fv} + \dot{m}_{ff} \quad (6)$$

into two parts. One part is the fuel vapour

$$\dot{m}_{fv} = (1 - X)\,\dot{m}_{fi} \quad (7)$$

that is carried with the air flow directly into the cylinder and the other part is the fuel that evaporates from the fuel film

$$\dot{m}_{ff} = \left(\frac{1}{\tau_{ff}}\right)\left(-\dot{m}_{ff} + X\,\dot{m}_{fi}\right) \quad (8)$$

on the intake manifold walls. The time constant τ_{ff} models the delay for the fuel vaporisation and X defines the fraction of the fuel that builds up the fuel film. To sum up the model, a differential equation for the engine speed

$$\dot{n} = -\frac{\left(P_f + P_p + P_b\right)}{(I\,n)} + \frac{\dot{m}_f\,H_u\,\eta_i\,(t - \tau_d)}{(I\,n)} \quad (9)$$

is defined. The first negative term in the equation defines the load P_b, the friction losses P_f and the pumping losses P_p. The second positive term represents the power generation from the fuel energy. H_u is the lower heating value of the fuel and η_i defines the thermal efficiency. The definition of

$$I = \frac{\left(\frac{2\,\pi}{60}\right)^2}{1000}\left(I_{eng} + I_{load}\right) \quad (10)$$

includes the inertia of the engine I_{eng} and the inertia of the load I_{load}. The time delay τ_d models transient behaviour after a fuel mass flow step. The before mentioned instantaneous engine variables, such as P_l, P_p, X, and η_i, are defined by

algebraic functions. The definitions of the algebraic functions are obtained from steady state engine measurements (Hendricks and Sorenson 1990, p.1883).

4.3.3 Engine process model

The most detailed model is based on the engine process model and represents the physical interrelationships, is a thermodynamic model and includes for example fluid dynamics for intake and exhaust, one or multiple-zone combustion models and wall heat transfer models. Furthermore the engine process model is suitable for implementation of submodels. These submodels are additional models and may be needed for the investigation of different phenomena, for example exhaust gas recirculation or knock behaviour. Contrary to the mean engine value model, that calculates mean values over one or more engine cycles, the engine process model calculates the change of variables during one engine cycle. It requires a big amount of input data and careful measurements, as well as correlation on a dynamometer. Correct parameters that are needed to adjust the models, can be extracted from collected data, for example for the wall heat transfer model. The outcome of such a calculation shows all losses in comparison to the perfect engine, split into the areas where they emerge. With this analysis it is visible how changes in combustion development or design affect different losses. After analysing the data, it is possible to identify the best compromise and thereby the direction of the development resulting in the least losses overall. The parametrization of this model is combined with a substantial effort. It is used mainly for engine development, but can also play a role in functional development of ECUs (Matthies 2013, p.39). A quasi-dimensional model approach is used to define the thermodynamic model. This means, an additional time dependent coordinate is introduced to represent geometrical relations without having an identified spatial location. Such an approach is needed to describe for example flame propagation (Caton 2016, p.22). Chmela, Pirker, and Wimmer (2014) state that using the first thermodynamic law, the cylinder can be described as an open system with the derivative of the mass conservation equation in respect to the crank angle φ.

$$\frac{dm}{d\varphi} = \frac{dm_e}{d\varphi} - \frac{dm_a}{d\varphi} - \frac{dm_{leak}}{d\varphi} + \frac{dm_f}{d\varphi} \tag{11}$$

Where m_e is the intake gas mass, m_a is the exhaust gas mass, m_{leak} the lost mass through leakage and m_f the fuel mass. Describing the cylinder as the control volume according to the energy conservation equation the derivative in respect to the crank angle φ yields

$$-\frac{pdV_{cyl,\varphi}}{d\varphi} + \frac{dQ_B}{d\varphi} - \frac{dQ_W}{d\varphi} + \frac{dm_e}{d\varphi}\, h_e - \frac{dm_a}{d\varphi}\, h_a - \frac{dm_{leak}}{d\varphi}\, h_a = \frac{dU}{d\varphi} \tag{12}$$

Where p is the cylinder pressure and $V_{cyl,\varphi}$ is the cylinder volume at the respective crank angle. The term $-\int pdV$ describes the pressure-volume work done on the system by the gas. The released energy by the fuel is defined by Q_B, and the entire term $dQ_B/d\varphi$ defines the combustion process. Due to the different temperatures of the gas and cylinder walls, a heat transfer takes place. The wall heat transfer is described with Q_W and the combination of the terms $dQ_B/d\varphi$ and $dQ_W/d\varphi$ represent the net heat release (Chmela, Pirker, and Wimmer 2014, p.636). The net heat release is an important term, as it defines the resulting cylinder pressure and therefore the gas force on the piston. The specific enthalpies are defined by h_e and h_a to form the terms that represent the respective enthalpy flows. The change of internal energy of the system is expressed by the term $dU/d\varphi$. To be able to calculate different states of the gas the ideal gas equation

$$p\,V = m\,R\,T \tag{13}$$

is derived in respect to the crank angle φ.

$$p\,\frac{dV}{d\varphi} + V\,\frac{dp}{d\varphi} = m\,R\,\frac{dT}{d\varphi} + m\,T\,\frac{dR}{d\varphi} + R\,T\,\frac{dm}{d\varphi} \tag{14}$$

With these main thermodynamic expressions a computation of the combustion process within an engine cycle is possible (Chmela, Pirker, and Wimmer 2014, p.637). Therefore one or multiple-zone models are developed. A single zone engine process model can be used for stoichiometric and lean running port injected engines. In case the air to fuel ratio is rich, unburned fuel is still present at the end of combustion and therefore needs to be modelled in a separate zone. These multiple-zone models provide additional information, for example about the

temperatures of the unburned and burned gases (Caton 2016, p.77). The respective terms in the equations have to be expressed through relationships or models. For example the heat transfer from the combustion gas to the cylinder walls is a complex phenomenon and several approaches exist. One of the most known models for the heat transfer coefficient

$$\alpha_G = 130 * d^{-0,2}\, p^{0,8}\, T^{-0,53}\, (C_1\, w)^{0,8} \tag{15}$$

was presented by Woschni and describes a model based on similarity theory and polynomial expressions (Chmela, Pirker, and Wimmer 2014, p.652). With the parameters d defining the cylinder bore, p the cylinder pressure and T the mean gas temperature. The constant C_1 changes its definition for the combustion cycle and for the low pressure cycle. Variable w describes the characteristic speed (Chmela, Pirker, and Wimmer 2014, p.652). A way to model the energy release of the fuel is the vibe function.

$$x_{br} = \frac{Q_B}{Q_{Btot}} = 1 - e^{\left[C*\left(\frac{t}{t_{tot}}\right)^{m_{vibe}+1}\right]} \qquad \varphi \in [360°, 540°] \tag{16}$$

The definition of the form factor m_{vibe} is used to manipulate the shape of the vibe curve. With t_{tot} the combustion total duration can be described. When the conversion rate Q_B/Q_{Btot} at $t = t_{tot}$ is set to 99,9%, then constant C becomes -6,908 (Pischinger, Klell, & Sams 2009, p.176).

4.4 Turbocharger models

Turbochargers are devices that use the exhaust gas energy to propel a compressor located on the intake side of the engine. The hot exhaust gas of an engine carries energy in form of enthalpy. This energy is used to spin the turbine which is connected through a shaft with the compressor. The compressor increases the intake air pressure and thereby also its temperature. To lower the temperature of the air before it enters the combustion chamber an intercooler is used. With the compressed and cooled down air, more oxygen is present and therefore more fuel can be injected. The boost ratio

$$a_{boost} = \frac{\rho_1}{\rho_0} \tag{17}$$

defines the increase in density of the charge and is representative for the increase in mean effective pressure and torque for constant air to fuel ratio (Pischinger, Klell, & Sams 2009, p.144). The variable ρ_1 defines the density at the intake valve and ρ_0 the density at ambient conditions. This concept can be used to produce more power from the same displacement or similar power from smaller displacement, called downsizing. Because the turbocharger relies on the exhaust gas massflow the performance is linked to the throttle position and engine speed. A spontaneous throttle opening during operation in low speed and load will cause a delayed torque delivery due to the exhaust gas massflow build up and the turbochargers inertia. To represent this turbocharger behaviour a medelling approach is needed. Similar to the possibilities of engine modelling there are several ways to replicate a turbocharger. In the following chapters an explanation of two models is given.

4.4.1 Torque delay model

As described before, torque build up on a turbocharged engine is slower than on a natural aspirated engine. The reason can be found in the mass and heat inertia of the turbocharger itself, but also in exhaust gas massflow build up with engine speed and load. Knowing the additional torque a turbocharger can provide, it is possible to model the delay with a proportional time element of first order (PT1) (Blundell and Harty 2004, p.358-359). This element is used for systems which can be described or approximated with a differential equation

$$T_{const}\,\dot{x}_a + x_a = x_e \tag{18}$$

of first order (Roddeck 2003, p.318). Solving the differential equation for x_a, the PT1 introduces a delayed signal depending on the magnitude of the time constant T_{const}. This method is the simplest way to represent a turbocharger lag. The input signal is defined as x_e and the output signal as x_a.

4.4.2 Thermodynamic model

A more complex approach is to model the turbocharger using thermodynamic equations. Starting with steady state definition of the pressure ratio between inlet and outlet, several influences like mechanical efficiency and heat transfer from turbine to the compressor can be accounted for (Isermann 2014, p.200-203). Isermann (2014) states that the compressor power

$$P_c = \dot{m}_c \frac{c_{pc}\, T_1^*}{\eta_{c,is}} \left(\left(\frac{p_2}{p_1} \right)^{\frac{\kappa_c - 1}{\kappa_c}} - 1 \right) \tag{19}$$

can be described by combining the enthalpy definition

$$\Delta h_{c,adi} = c_{pc} \, (T_2^* - T_1^*) \tag{20}$$

of the inlet and outlet temperatures. With $\dot{m}_c$ describing the compressor massflow. T_2^* is the temperature and p_2 the pressure at the compressor outlet. T_1^* and p_1 are the compressor entry temperature and pressure. The isentropic exponent is expressed through κ_c and c_{pc} is the specific heat capacity of the intake air. Using the isentropic compressor efficiency

$$\eta_{c,is} = \frac{\left(\frac{p_2}{p_1} \right)^{\frac{\kappa_c - 1}{\kappa_c}} - 1}{c_{pc} \left(\frac{T_2^*}{T_1^*} - 1 \right)} \tag{21}$$

the flow friction is accounted for. The values for p_2/p_1 and the isentropic efficiency coefficient $\eta_{c,is}$ are obtained from stationary compressor maps which depend on the corrected massflow $\dot{m}_{c,cor}$ and the corrected turbocharger speed $n_{tc,cor}$. The corrected variables are used to eliminate the dependency on changing environmental conditions when measuring the maps. The same modelling approach can be used on the turbine and therefore the turbine power

$$P_{t,adi} = \dot{m}_t \, c_{pt} \, T_3^* \, \eta_{t,is} \left(1 - \left(\frac{p_4}{p_3} \right)^{\frac{\kappa_t - 1}{\kappa_t}} \right) \tag{22}$$

expressed. With $\dot{m}_t$ describing the turbine massflow and p_4 the turbine exit pressure. T_3^* and p_3 are the turbine entry temperature and pressure. The isentropic exponent is expressed through κ_t and c_{pt} is the specific heat capacity of

the exhaust gas. To obtain the turbocharger dynamics the equation for equal angular momentum

$$J_{tc}\,\frac{d\omega_{tc}}{dt} = M_t - M_c - M_f \tag{23}$$

is used. Where J_{tc} defines the turbocharger inertia and ω_{tc} the turbocharger speed. The turbine torque is represented by M_t, the compressor torque by M_c and the friction torque by M_f (Isermann 2014, p.194-200). This turbocharger model requires inputs like intake massflow, temperatures and pressures and therefore defines the state of a substance. Because the thermodynamic turbocharger model uses the same modelling approach as the mean value engine model, it is suitable for implementation. The lookup table engine model does not provide substance states without additional calculations, and therefore this turbocharger model is not suited for implementation there.

4.5 Friction models

Friction occurs in every moving part and can influence the performance of the desired movement significantly. But friction is also wanted when forces need to be transmitted. Without the friction force no tire would grip and no clutch could operate. Looking deeper into this topic reveals that friction generation and the transition between sticking and slipping is a complicated process. The basic and most known expression of the friction force

$$F_R = F_N\,\mu \tag{24}$$

described by Coulomb is a dependency on a perpendicular normal force F_N and friction coefficient μ **Figure 7a)** (Olsson 1996, p.25). With this simple model the friction force F_R is opposed to the external force, is not changing with velocity and is equal to the external force when the velocity is zero. With Reynolds friction force caused by the viscosity of fluids developed a velocity dependent friction description **Figure 7b)**. But the viscous friction does not always change linearly with the velocity, a more detailed description of the friction force shows **Figure 7d).** In reality when an object is at rest the static friction (stiction) has to be described dependent on the acting force and not on velocity. If the acting

force is large enough the static friction force can not prevent the object from moving (Olsson 1996, p.26-27).

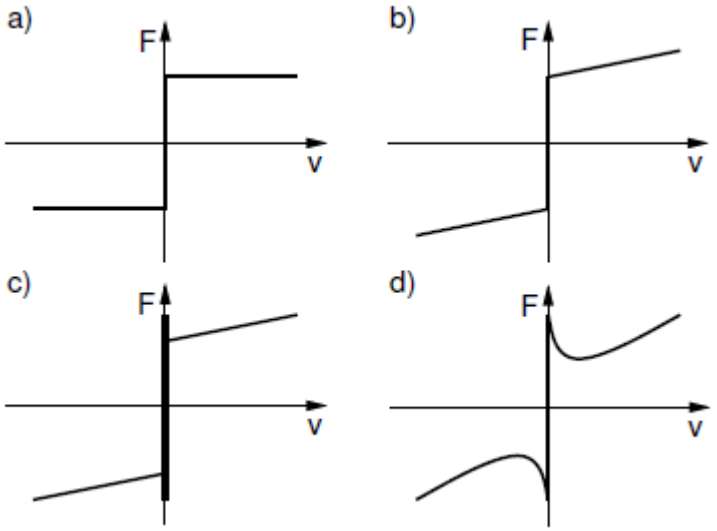

Figure 7: a) Coulomb friction, b) couloumb with dynamic friction, c) Coulomb with stiction and reduced dynamic friction and d) Coulomb with improved dynamic friction (Olsson, p.27)

However, as mentioned before with these models the friction force is not defined at zero velocity and causes numerical problems. To overcome this problem a solution could be using a very steep gradient to reach maximum Coulomb friction. Following this idea it is possible to use a tanh function as shown in **Figure 8**.

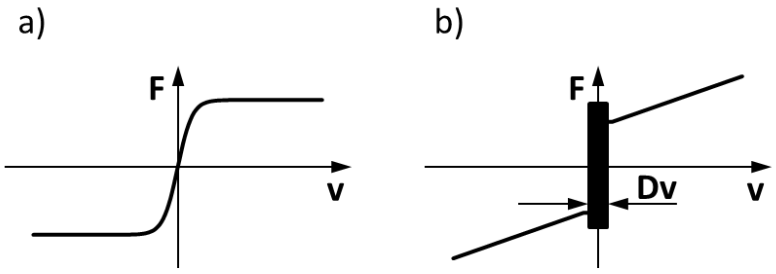

Figure 8: a) tanh friction description, b) Karnopp model with intervall D_v

The disadvantage of using the modelling approach is that there is no real sticktion behaviour. The torque output can be correlated to be correct but there will always be residual speed. Another possibility was proposed by Karnopp. Instead of having an undefined friction force at zero velocity, the Karnopp model

$$F_R = \begin{cases} F_{ext} & ,for\ |v| \leq D_v \wedge |F_{ext}| < \mu_s F_N \\ \mu_s F_N\ sign(F_{ext}) & ,for\ v = 0 \wedge |F_{ext}| \geq \mu_s F_N \\ F_D(v) & ,else \end{cases} \quad (25)$$

uses a velocity interval D_v (Gradowhl, Belšak, & Hirz 2017, p.11). Where F_R is the resulting friction force, F_{ext} is the external acting force, μ_S is the static friction coefficient, F_N is the normal force on the friction surface and $F_{D(v)}$ is the dynamic friction force. A numeric solution would never calculate exactly zero velocity and as a result of that, constantly oscillate around zero. This would cause continuous transitions from sticking to slipping and thereby numeric noise. With a deadzone defined, in case the numeric solution calculates a value near zero velocity and if this value is within this deadzone D_v, the modell will output zero velocity **Figure 8**. The Karnopp friction model has a low calculation time and is therefore used for real time simulations. None of the models so far takes the change in velocity into account. Many experiments have shown a clear hysteresis depending on increase or decrease of velocity as well as friction behaviour that the static models can not reproduce. With higher demands on control systems better friction models, so called dynamic models, were needed (Olsson 1996, p.29-30). Several models were introduced based on the microscopical contact between two surfaces (Olsson 1996, p.29-30). Two of them are the Dahl and LuGre model. They are able to describe the preslide effect, a deformation and therefore a relative movement without breaking into sliding. The LuGre is based on a bristle model as shown in **Figure 9**. The bottom bristles can be thought as rigid for better imagination.

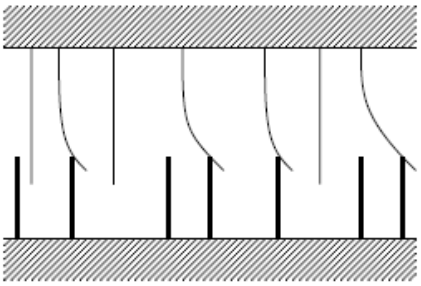

Figure 9: Visualisation of a bristle model (Olsson, p.45)

The model uses parameters to describe the bristle stiffness and damping rates. Sticking is described while the top and bottom bristles interlock with each other. One can imagine the preslide deformation when the bristles begin to bend. Transition from sticking to slipping is described when the top bristles start to move over the bottom ones. With the possibility to parametrise the damping rate of the bristles, the resistance of the bristles becomes velocity dependant. With a velocity dependant damping rate, it is possible to depict the before mentioned friction dependency on velocity change. Additional to that, the parametrisation can be asymmetric and thereby depict different behaviour for positive and negative velocity changes. Olsson (1996) describes the LuGre friction model

$$\frac{dz}{dt} = v - \frac{|v|}{g(v)}\, z \tag{26}$$

$$g(v) = \frac{1}{\sigma_0}\left(F_c + (F_s - F_c)e^{-\left(\frac{v}{v_s}\right)^2}\right) \tag{27}$$

$$F_r = \sigma_0\, z + \sigma_1(v)\, \frac{dz}{dt} + F_v\, v \tag{28}$$

$$\sigma_1(v) = \sigma_1\, e^{-\left(\frac{v}{v_d}\right)^2} \tag{29}$$

with four mathematical relations. The earlier mentioned bristle stiffness is described as σ_0. The dynamic bristle damping rate is represented by $\sigma_1(v)$, and is dependent on the differential velocity v between the friction surfaces. F_C and F_S describe the Coulomb and static friction force, dependent on the friction coefficients μ_C and μ_S and the normal Force F_N. F_V would represent the viscous

friction part for lubricated systems but is not used in this case of application because the system is a dry clutch. The parameter v_s describes the Stribeck velocity and defines where the Stribeck effect is pronounced. The Stribeck effect describes the increase of friction force with decreasing velocity for low velocities (Olsson 1996, p.11). The definition of v_d describes the velocity range for the damping to be active around zero velocity (Olsson 1996, p.63). With this parameters defined the virtual bristle bending z can be calculated and thereout its bending velocity dz/dt. This deflection of a single bristle can be imagined as the average deflection of all bristles (Olsson 1996, p.46) and is shown in **Figure 10**.

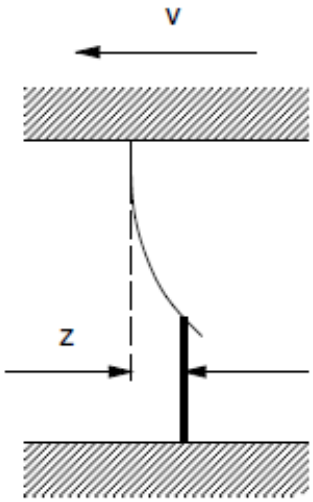

Figure 10: Average bristle deflection z due to velocity v between the friction surfaces

Summing up it can be noted that by using the LuGre model it is possible to replicate many friction phenomena, the difficulty is to find the correct parameters and validate the model. In terms of calculation time the LuGre model is slower than the other presented models especially compared to the Karnopp, that takes only small recourses to calculate but often deliver sufficient results (Bataus 2011, p.116).

5 Modelling

In this chapter the model building in Simulink is described, and it is mentioned why one method was chosen over another one and the most important input parameters are shown.

5.1 Model breakdown

The vehicle model is divided into following submodels

- Engine
- Engine control unit (ECU)
- Clutch
- Transmission
- Transmission control unit (TCU)

Partitioning the model this way is an attempt to represent the real parts as much as possible and to display data flow, for example torque interventions from the Transmission control unit (TCU) to the Engine control unit (ECU). A further advantage is the possibility to reuse the submodels in other applications. For example the submodel of the clutch can be used in an entirely different powertrain model. Each model can also be tested in an isolated environment to investigate its behaviour and correlate the submodel with the behaviour of the respective real component. This allows for early stepwise model verification without the necessity to have the entire powertrain available as hardware, which would be used to perform tests on, analyse the results and use them to correlate the simulation models. What also needs to be considered is the fact, that not just one manufacturer develops and produces all components. Therefore test data from different manufacturers is available at a different time. Already available test data, for example from early prototype tests, can be sent to the simulation model developer to verify the submodels.

5.2 Engine

To choose the right type of model for the engine simulation, it is necessary to define the requirements for shift behaviour simulation. The model should be able to depict the dynamic properties of the real engine. Ideally this means not only averaged torque or revolution figures, but also pulsations and oscillations over a crankshaft rotation as they can have an influence on the system. As mentioned before, an engine process model is needed for combustion development and other detailed investigations for engine design, it is not considered as an option. A mean value model is also too complex and requires much data, that is not available, to correlate with the real motor. Compared to the look up table model the calculation time is high because several thermodynamic equations and other physical relationships have to be solved. The lookup table model does not need to calculate torque production but simply reads it out of a table. With additional delays the look up table model is able to depict up to a certain level of accuracy the dynamic behaviour of an engine (Matthies 2013, p.37). The limitations of the model are the not present thermodynamic relationships, and therefore complex physical processes have to be mathematically approximated. For the purpose of shift behaviour investigations, a realistic torque source is required and an improved look up table model is capable of providing one (Matthies 2013, p.36).

5.2.1 Improved look up table model

The powerunit modelled in this work is a turbocharged 6 cylinder gasoline engine. In this thesis not only the mean torque delivery is modelled, but also torque pulsations and oscillations over crankshaft revolutions. This means the pulsations are depending on firing order, number of cylinders, and if it is a v-shaped engine, on the bank angle. Starting with cylinder one as origin and φ at 0° in its top dead centre (TDC) the other cylinders have the correct offset to their respective TDC. Each cylinder has its own φ_i and can be combined into a bus system φ_{bus}. This bus is used as an input for all torque generation blocks, hence an output torque is calculated for each cylinder respectively. Therefore the origin of torque can be divided in different parts.

- Oscillating masses
- Gas force on the piston without combustion
- Gas force on the piston with combustion

The following chapters explain the origin of these forces and how they can be implemented in the model.

5.2.1.1 Force on piston due to oscillating masses

Rotating and oscillating masses of an engine include piston, piston pin, connecting rod, crankshaft and the valvetrain. When an engine is turning, the oscillating parts are constantly accelerated and slowed down because of a linkage transforming the translatory motion of the pistons into the rotatory motion of the crankshaft. The piston position

$$s_{pist} = r\left(1 + \frac{1}{\lambda_{cr}} - \cos(\varphi) - \frac{1}{\lambda_{cr}}\sqrt{1 - {\lambda_{cr}}^2\ \sin(\varphi)^2}\right) \tag{30}$$

in relation to the crank angle results from the kinematics (Urlaub 1989b, p.9). The second derivative of the piston position in respect to time yields in the piston acceleration $\ddot{s}_{pist}$. This alternating positive and negative acceleration results in an oscillating translational force F_m. The calculation

$$F_m = \left(m_{pist} + m_{cr}\right)\ddot{s}_{pist}(\varphi) \tag{31}$$

takes into account the piston mass m_{pist}, including piston pin, and the oscillating part of the conrod m_{cr}. It is common to approximate the square root in (30) with a Maclaurin series. This approximation shows that the Alternating force from (31) is a sum of different order forces with different magnitudes. The approximation is usually aborted after the second order and using trigonometric relations yields in the approximated piston position.

$$s_{pist} \approx \left(1 + \frac{\lambda_{cr}}{4} - \cos(\varphi) - \frac{\lambda_{cr}}{4}\cos(2\,\varphi)\right) \tag{32}$$

It is possible to calculate the approximated oscillating forces as shown in (31) by forming the second derivative

$$\ddot{s}_{pist} \approx r_{cs}\,\omega^2\,(\cos(\varphi) + \lambda_{cr}\ \cos(2\,\varphi)) \tag{33}$$

of the approximated piston position in respect to time. It is visible from (33), that the second order force oscillates with double the frequency *(2 φ)* of the first order force *(φ)* and is smaller in magnitude. With the numerical solutions the root term is modelled and all orders are included in the solution. **Figure 11** shows the torque at the crankshaft for each cylinder caused by the oscillating masses at a given engine speed. Assuming the crankshaft as stiff, the combination of all torques will result in a slightly smaller overall amplitude for this engine configuration.

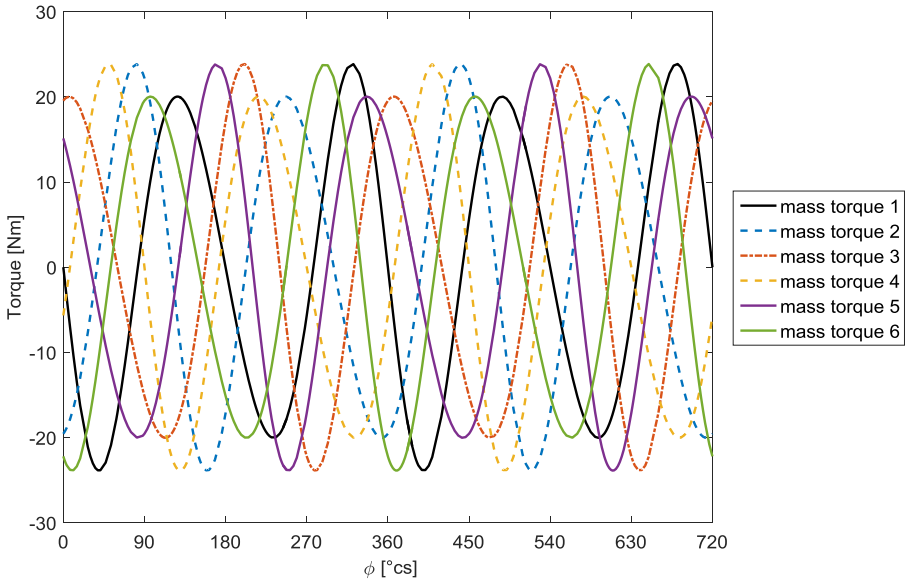

Figure 11: Oscillating mass inertia torque at the crankshaft cylinderwise, n_{eng} = 4000 n/min, load = 20 %

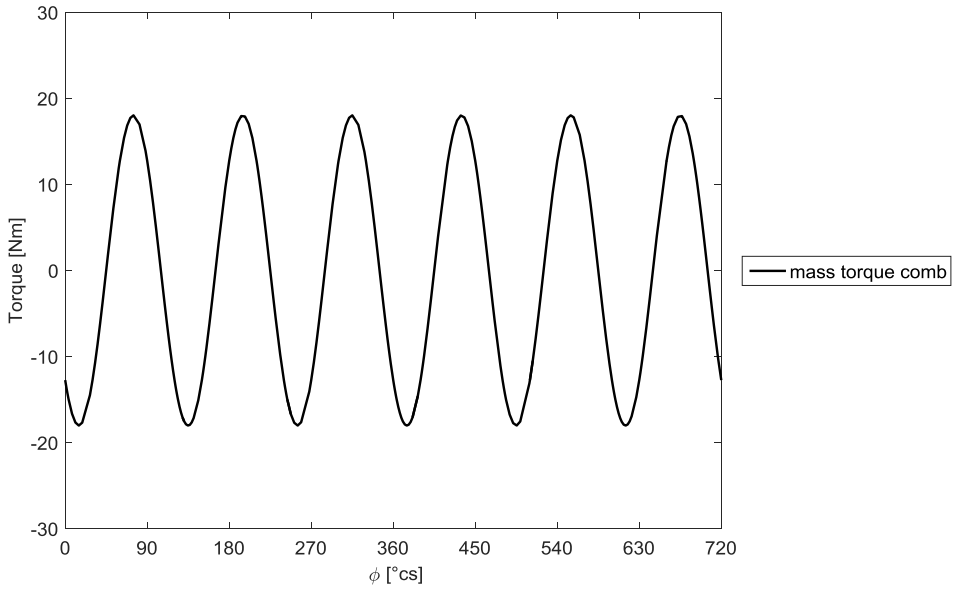

Figure 12: Combined oscillating mass inertia torque at the crankshaft, n_{eng} = 4000 n/min, load = 20 %

5.2.1.2 Gas force on piston without combustion

When the engine is in the charge exchange phase its pistons pull fresh air or air-fuel mixture into the combustion chamber while the inlet valves are open. As soon as the inlet valves close and the piston is in its upward motion towards the TDC a compression takes place. The modelling of compression and expansion in this work is based on the thermodynamic polytropic process.

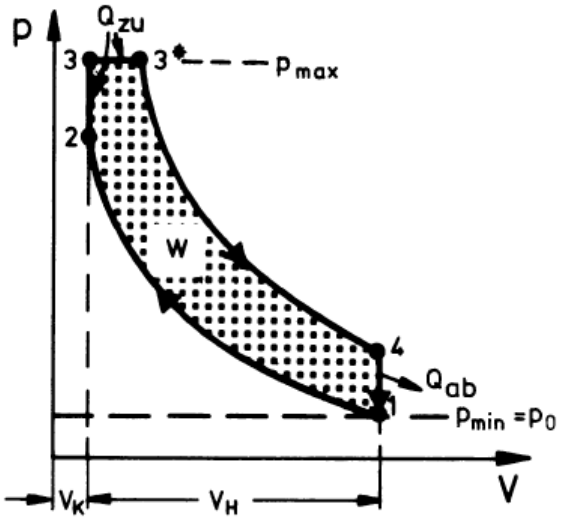

Figure 13: Ideal thermodynamic cycle of a gasoline engine (Urlaub 1989a, p.14)

The ideal thermodynamic dual cycle uses the following assumptions and approximations:

- 1-2 isentropic compression (adiabatic and reversible)
- 2-3 isochoric heat addition (heat release due to combustion)
- 3-3* isobaric heat addition (heat release due to combustion)
- 3-4 isentropic expansion
- 4-1 isochoric heat subtraction (exhaust heat)
- Neither an inlet or outlet gas displacement is included

The calculated results of these ideal cycles are too optimistic in comparison to real engines especially the work, torque and power. This deviance results mainly from heat addition instead of a combustion process, the adiabatic and reversible compression and expansion and the missing gas exchange (Caton 2016, p.20-21). But nevertheless, they can predict the trends of important engine characteristics (Caton 2016, p.20). This idealised process assumes the compression start at $\varphi = 180°$ (BDC). After passing the TDC and without any combustion an expansion takes place until the exhaust valves open, based again on the ideal assumption at $\varphi = 540°$. These gas pressure

$$p_{cyl,lp}(\varphi) = \left(\frac{V_{cyl,0}}{V_{cyl,\varphi}}\right)^{n} p_{cyl,0} \qquad \varphi \in [180°, 540°] \qquad (34)$$

$$p_{cyl,lp}(\varphi) = p_{cyl,0} \qquad \varphi \in [0°, 180°], [\,540°, 720°] \qquad (35)$$

act on the piston and is modelled by a polytropic compression and expansion. With $p_{cyl,0}$ and $V_{cyl,0}$ defining the cylinder pressure and volume at compression start. $V_{cyl,\varphi}$ defines the actual cylinder volume. As mentioned before the isentropic process causes differences in the pressure $p_{cyl,lp(\varphi)}$ at the end of the process. To improve this assumption the polytropic process can be used as it takes the heat transfer into account. Merker, Schwarz and Teichmann (2009) state, that the polytropic exponent can be estimated as constant between particular crankshaft angles. This assumption is used to estimate the pressure level in cylinder pressure measurement and proposes the value for gasoline engines $n=1,32\text{-}1,33$ (Merker, Schwarz and Teichmann 2009, p.67). Index 0 defines the states at the beginning of the compression (Isermann 2014, p. 182). With the pistons projected area the low pressure gas force

$$F_{g,lp}(\varphi) = p_{cyl,lp}\, A_{bore} \qquad \varphi \in [180°, 540°] \qquad (36)$$

acting on the piston can be calculated. The cylinder cross section is expressed through A_{bore}. **Figure 14** shows the torque at the crankshaft caused by the gas forces without combustion.

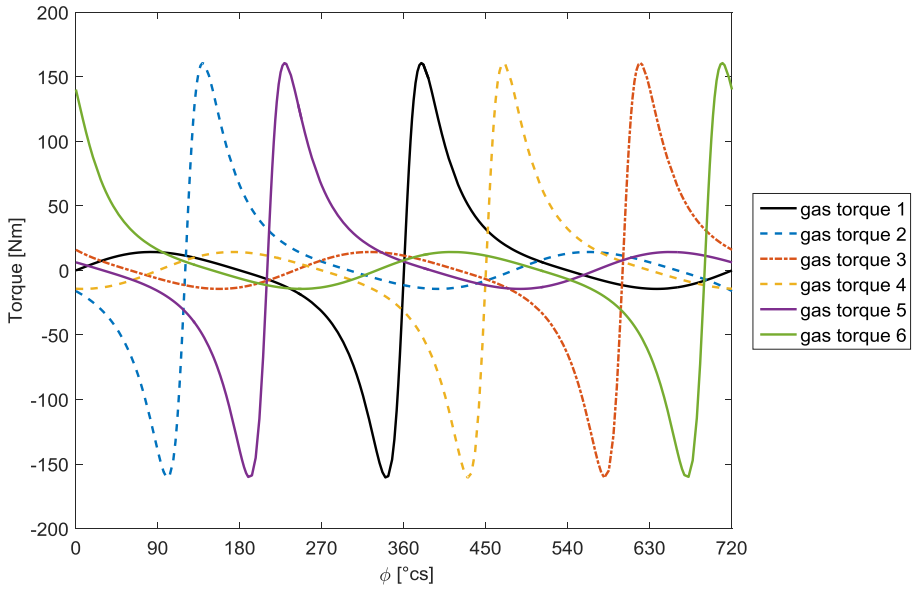

Figure 14: Compression and expansion torque cylinderwise, n_{eng} = 4000 n/min, load = 20 %

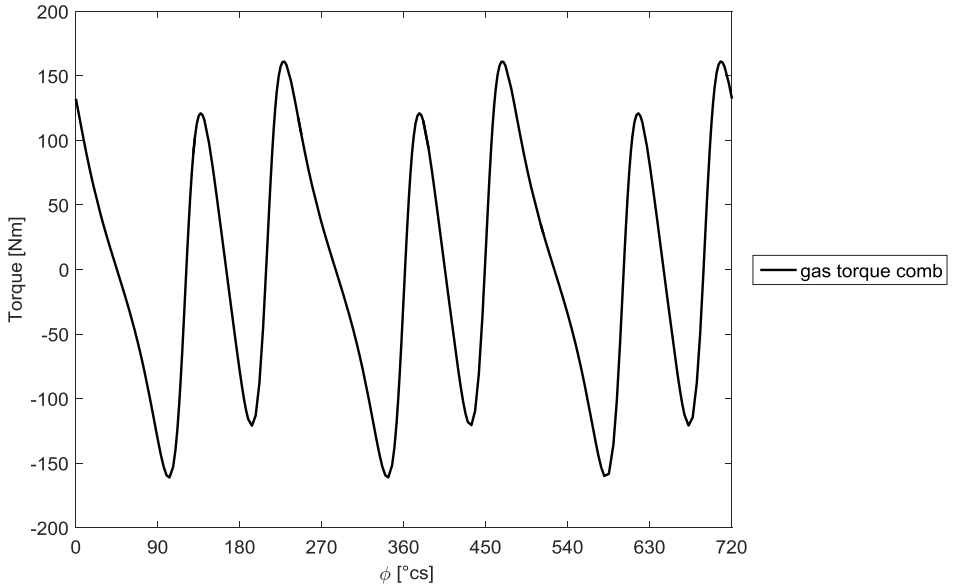

Figure 15: Compression and expansion torque, n_{eng} = 4000 n/min, load = 20 %

5.2.1.3 Gas force on the piston due to combustion

After the low pressure cycle compression is finished the combustion, in case of a gasoline engine it is initiated through a spark, takes place. The burning air-fuel mixture causes a high pressure curve, until the outlet valves are opened. This combustion is often expressed by an empirical model, with the burn rate approximated by a vibe curve as described in the theoretical part of this thesis. With this approximation it is possible to calculate the heat release curve, but not the cylinder pressure because of the wall heat losses. To estimate the wall heat losses another model is needed, for example the empirical model of Woschni. Both models would need engine tests to correlate their behaviour and give satisfying results. As this is not an option for this model build in the present work, a simpler solution needs to be found. With an existing torque map the average cylinder pressure is known, and with the vibe function transformed to torque at the crankshaft

$$M_{g,comb}(\varphi) = a\,\varphi'^2\,e^{(-b\varphi')} \qquad \varphi \in [360°, 540°] \tag{37}$$

$$\varphi' = \varphi - 360° \tag{38}$$

a reverse engineered generic torque curve can be generated with its functional limits being TDC and BDC (Isermann 2014, p. 184). Instead of calculating the resulting cylinder pressure, this approach takes the already indirectly known mean indicated pressure through the known engine torque map and recreates a combustion torque curve. With the parameter defining the crankshaft angle for maximum torque φ_{max}, also the shape of the torque curve changes to maintain the mean torque over one engine cycle. Taking into account the torque produced by gas force without combustion $M_{g,lp}$ and the torque due to mass inertia of the oscillating parts M_m,

$$M_{basic} = M_{g,lp} - M_m \tag{39}$$

is defined. Averaged over two crankshaft rotations the combined engine torque has to equal the indicated mean engine torque from the torque map

$$\frac{1}{720°}\int_{0°}^{720°} M_{g,comb}(\varphi)\,d\varphi = \bar{M}_{eng,i} \tag{40}$$

because

$$\bar{M}_{basic} = 0 \tag{41}$$

The crank angle of the maximum torque

$$\frac{d}{d\varphi'} M_{g,comb}(\varphi) \Big| \varphi' = \varphi_{max} = 0 \tag{42}$$

is assumed constant (Sinsel 2000). With (40) and (42) the parameters

$$a = \frac{4 * 720° * \bar{M}_{eng,i}}{(\varphi'_{max})^3} \tag{43}$$

$$b = \frac{2}{\varphi'_{max}} \tag{44}$$

from (37) can be defined (Isermann 2014, p. 183-184). The mean indicated engine torque is defined by $\bar{M}_{eng,i}$. With φ_{max} being the single parameter to define, this approximation of the pulsations caused by combustion is much simpler than the method with modelling the net heat release. Isermann (2014) describes and shows in several figures the good approximation of this method within his work. The resulting torque at the crankshaft using this approximation shows **Figure 17.** The approximation shown by Isermann (2014) delivering good results with $\varphi_{max}=12°$ is for a truck diesel engine. Comparing measurements of cylinder pressure between a truck diesel engine and a passenger car gasoline engine, as shown in **Figure 16**, it is visible that the maximum pressure of the truck diesel engine is at a lower crank angle. Taking this into account and the fact that the powerunit described in this work is for a sportscar, the assumption is made that the combustion duration is shorter than showed in **Figure 16** for the passenger car. With a shorter combustion duration the peak pressure moves to lower crank angles to achieve the same crank angle for 50% fuel mass fraction burned. Therefore the estimation is made with $\varphi_{max}=15°$ for this work. This assumption needs to be verified when engine test data is available.

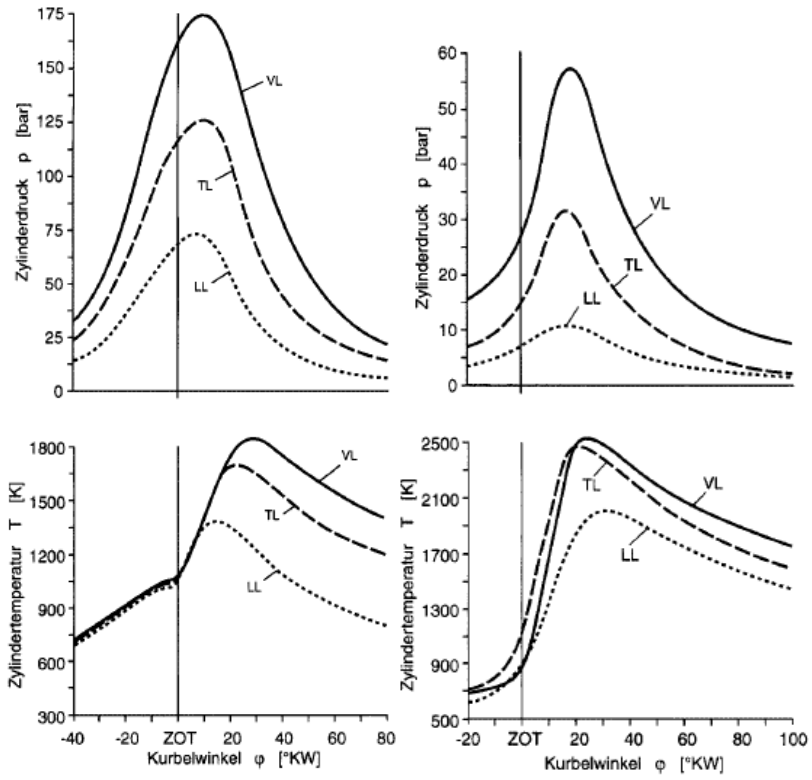

Figure 16: Comparison truck diesel engine with passenger car gasoline engine (Pischinger, Klell, & Sams 2009, p.365-372)

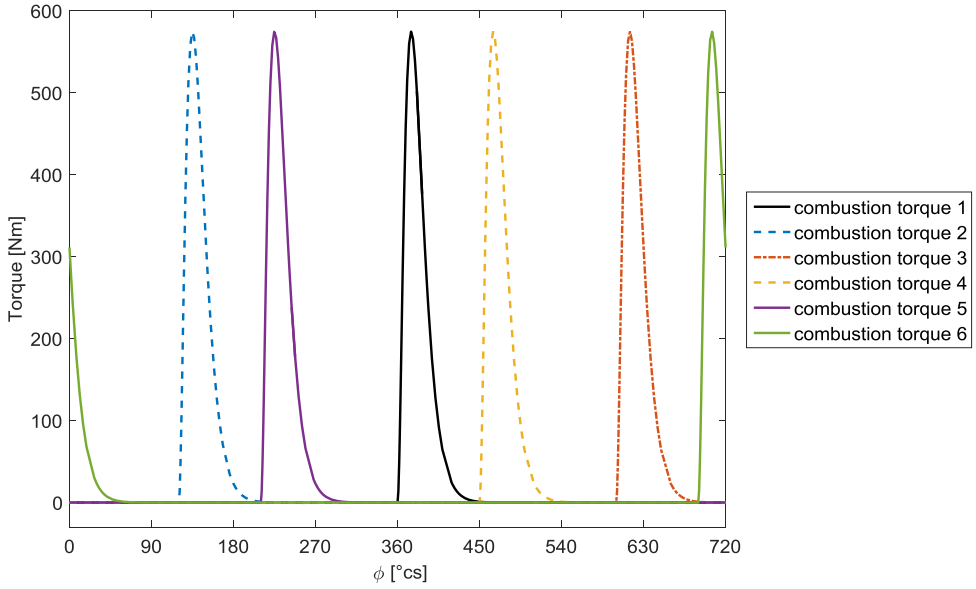

Figure 17: Combustion torque approximation cylinderwise, n_{eng} = 4000 n/min, load = 20 %

5.2.1.4 Friction torque

The friction torque for a given engine with oil at operating temperature is dependent on engine speed and load. Different engine parts have different dependencies, some are quadratic and others are linear. With no reference values it is possible to assume a mean friction pressure

$$p_{mr} = p_{mi} - p_{me} \tag{45}$$

$$p_{me} = p_{mi}\eta_m \qquad \eta_m = 0{,}85 \ldots 0{,}90 \tag{46}$$

to calculate the friction torque

$$M_r = \frac{p_{mr}\, V_d}{4\,\pi} \tag{47}$$

acting on the crankshaft. With p_{mi} describing the mean indicated pressure, p_{me} the mean effective pressure and η_m the mechanical efficiency coefficient. Schreiner (2015) states, that without measurement data for friction, an estimation can be made by a look up table depending on load and speed. To roughly reflect the different dependencies on engine load and speed a simple approach

$$\frac{p_{mr}}{p_{mr,full\_load}} = \frac{2}{3} * \frac{n}{n_{full_{load}}} + \frac{1}{3} * \frac{p_{me}}{p_{me,full\_load}} \tag{48}$$

can be implemented (Schreiner 2015, p.105).

5.2.1.5 Resulting engine torque

With all significant torque sources defined it is possible to model the produced engine torque. The gas and mass inertia forces on the piston need to be converted to torque acting on the crankshaft. This is done by geometrical relations

$$F_t(\varphi) = F_{pist}(\varphi)\left(\sin(\varphi) + \frac{\lambda_{cr}\ \sin(2\varphi)}{2\sqrt{1 - {\lambda_{cr}}^2\ \sin(\varphi)^2}}\right) \tag{49}$$

$$M_{pist}(\varphi) = F_t(\varphi) r_{cs} \tag{50}$$

of the cranktrain (Urlaub 1989b, p.14). Combining all torques

$$M_{eng} = M_{g,comb} + M_{g,lp} - M_m - M_r \tag{51}$$

results in the final engine torque. **Figure 18** depicts the resulting torque for one cylinder and all the modelled components. **Figure 19** shows the resulting engine torque at the crankshaft. To visualise the changing mass torque with engine speed two torque curves are shown in **Figure 20.** With the same throttle opening the combustion torque increases just slightly, much more dominant is the change in torque due to the oscillating masses. The change in load but at the same engine speed is shown **Figure 21**. It is visible that only the combustion torque has an influence on the shape of the torque curve. Because the pressure at the beginning of the compression $p_{cyl,0}$ is constant, the torque due to gas pressure without combustion does not change. An improvement could be made with a throttle position and engine speed dependant pressure $p_{cyl,0}$.

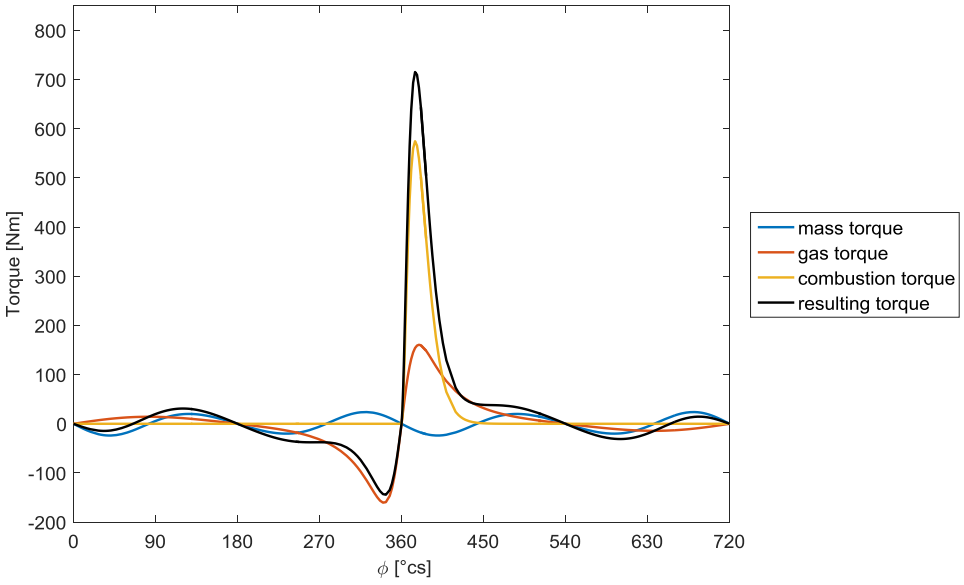

Figure 18: Resulting torque and its components for one cylinder, n_{eng} = 4000 n/min, load = 20 %

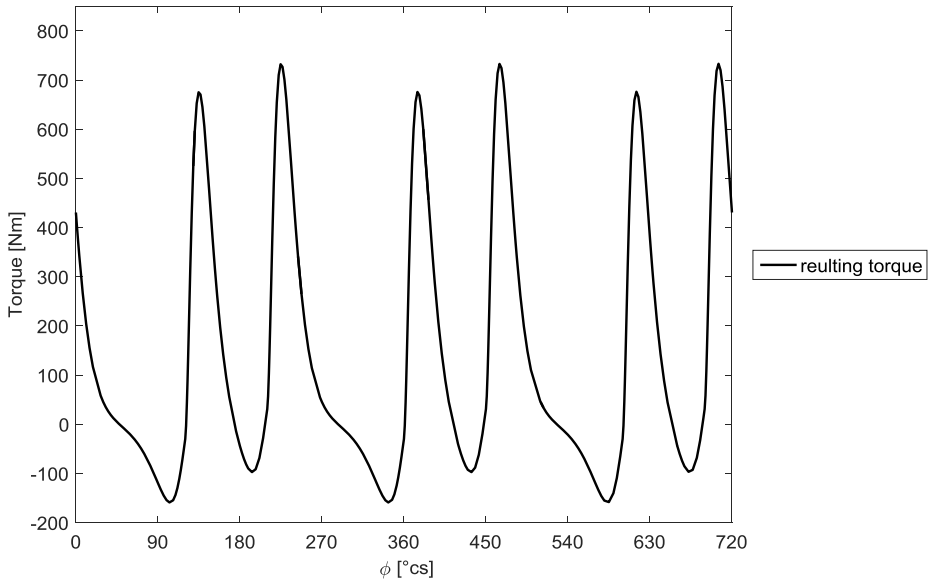

Figure 19: Engine torque, n_{eng} = 4000 n/min, load = 20 %

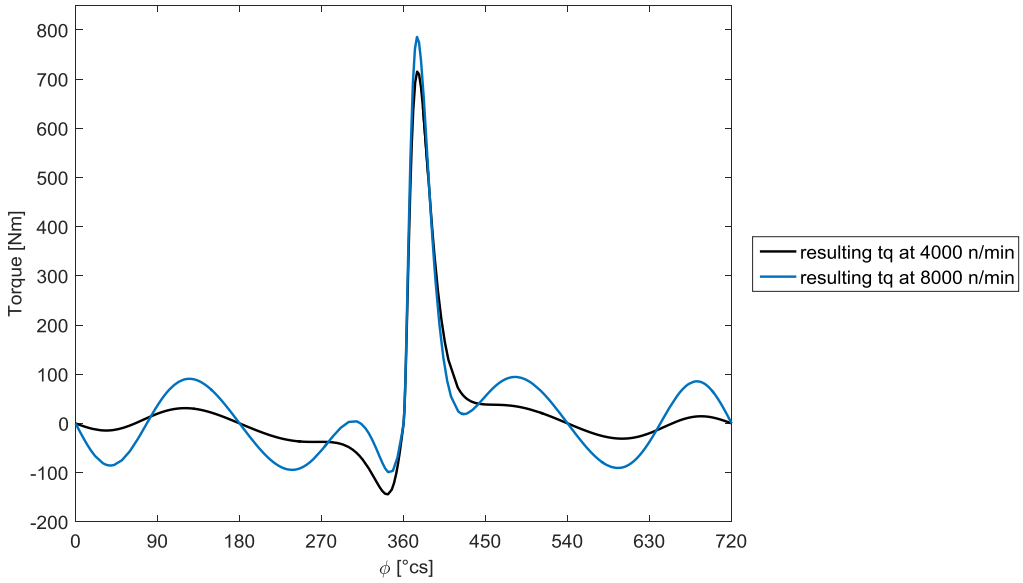

Figure 20: Engine torque at different speeds for one cylinder, load = 20 %

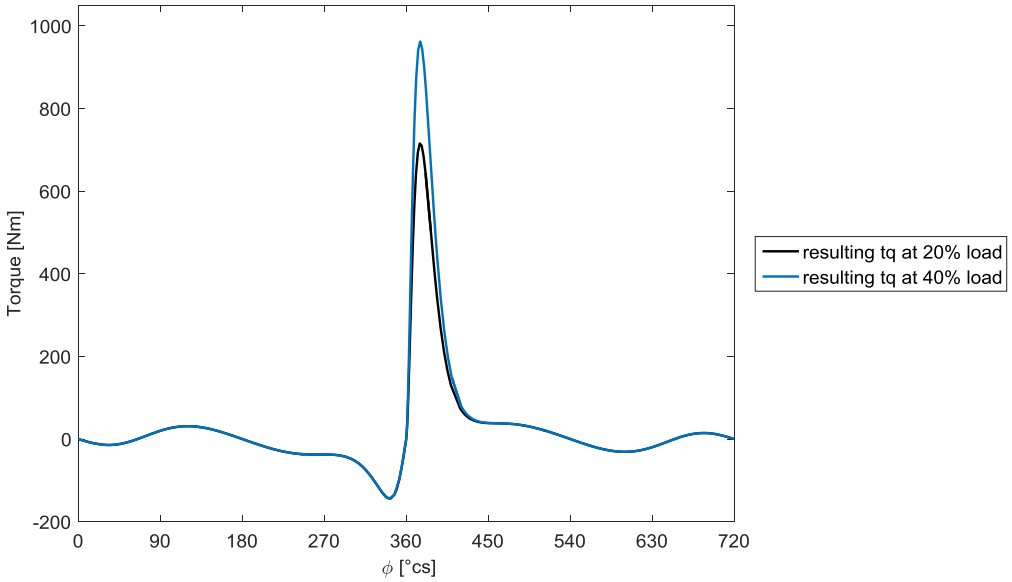

Figure 21: Engine torque at different load for one cylinder, n_{eng} = 4000 n/min

5.2.1.6 Engine and turbocharger torque map

As described in the previous chapter, the combustion torque calculation uses an engine torque map as an input. Ideally this map would be created from engine cylinder pressure measurements on a test bed. Unfortunately this information is not available, therefore both maps, one for the engine and one for the turbocharger torque, were assumed. The engines maximum speed and an estimated power figure were known. A similar high revving single cylinder engine torque map was available. Park, Matsumoto, and Oda (2010) state that downsizing for approximately 30% delivers similar engine power. The turbocharger modelled in this thesis is electrically supported and therefore can be designed bigger without the disadvantage of insufficient response time. Taking this information into account an additional 35% to the naturally aspirated power can be assumed. Using this information an artificial torque curve with a similar shape as the single cylinder power curve was designed. The maximum power value of this artificial naturally aspirated power curve is 35% below the known maximum power figure of the 6 cylinder engine. An additional torque curve was

modelled to represent the turbocharger torque similar to the shape showed in **Figure 22**.

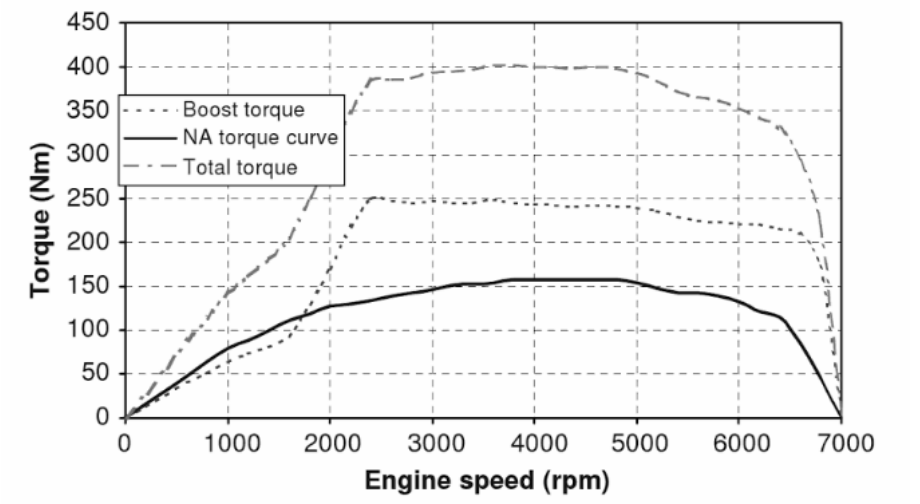

Figure 22: Torque curve for naturally aspirated engine operation, additional turbocharger torque and combined torque (Blundell and Harty 2004, p.360)

From the before mentioned single cylinder also a measurement of torque over throttle angle and speed was available. Normalising the torque curve at 100% throttle position, shows the relations of the torque reduction over speed for the respective constant throttle angles. Thereby the normalized torque at 100% throttle angle is constantly 1. The speed band is expressed through speed step samples and is thereby also normalised. A function was developed to model the normalised curves.

$$y = k \cos\left(\pi \frac{s_i}{s_{tot}}\right) + d \tag{52}$$

Where y is the output of the function, k is a scaling factor and d an offset fitting factor. The variable s_i defines the used sample and s_{tot} the total amount of the speed samples. The correlation of the function is shown in **Figure 23** for the throttle position at 20%, 30% and 50%.

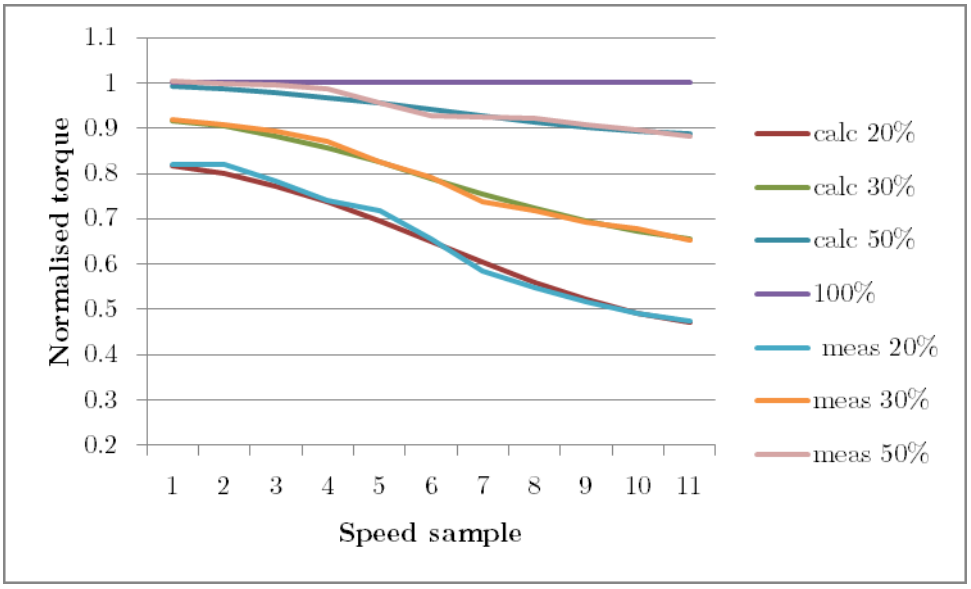

Figure 23: Approximation of torque reduction over speed and constant throttle angle

The previously designed torque curves for the engine and turbocharger can now be multiplied with the output values y of this function and the interpolated speed samples to match the speed band of the 6 cylinder engine. By multiplying the curves with the function the finished torque maps over speed and throttle angle are obtained.

5.2.1.7 Average speed and torque calculation

The engine inertia is estimated by the manufacturer and provided as a lumped inertia value. It includes the crankshaft inertia and the transformed inertia for the valvetrain and flywheel. The modelling approach for torque oscillations causes the engine speed to oscillate. When feeding the oscillating speed signal directly from the crankshaft as an input to the torque look up table, the torque output is not correct. To overcome this problem, an average engine speed over two crankshaft rotations is calculated. By doing this the speed signal is smoothened and can be used as an input to provide proper torque output from the look up table.

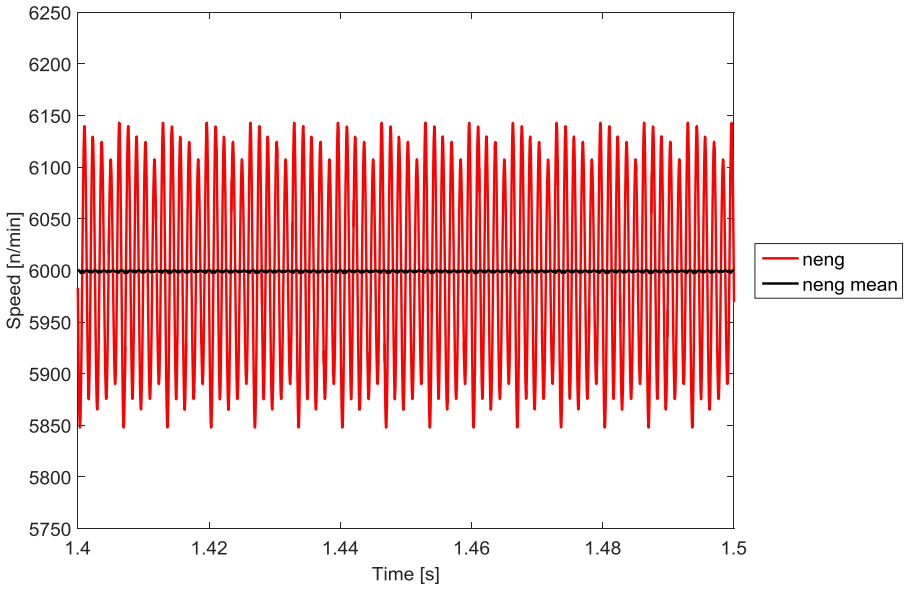

Figure 24: Averaged engine speed signal

5.2.1.8 System delay modelling

To replicate the transient behaviour of the engine several delays need to be implemented. When the desired throttle angle signal reaches the throttle valve actuator, it takes a certain time to actually reach this throttle angle because of inertia of the entire system. **Figure 26b)** makes the modelled delay visible. For this and also the following delays described proportional time elements of first order (PT1) are used as described in the theoretical part of this thesis. In the simulation model another delay occurs after the throttle valve reached its final position. Gas dynamics in the intake system prevent an instantaneous change of mass flow. This replicated behaviour describes **Figure 25a)** as spontaneous engine torque delay. Additional to that, yet another delay takes place when the throttle is opened while the intake valves are still closed. This time difference is modelled as the time for half a crankshaft rotation and is visible in **Figure 26a)** as engine torque dead time. As the engine speed is not constant a variable time constant of the PT1 element depending on engine speed is used. In the same way the intake filling delay can be modified, also taking into account the load at the time being for more realistic behaviour. An explanation for the approximation of the used values is given in the next chapter.

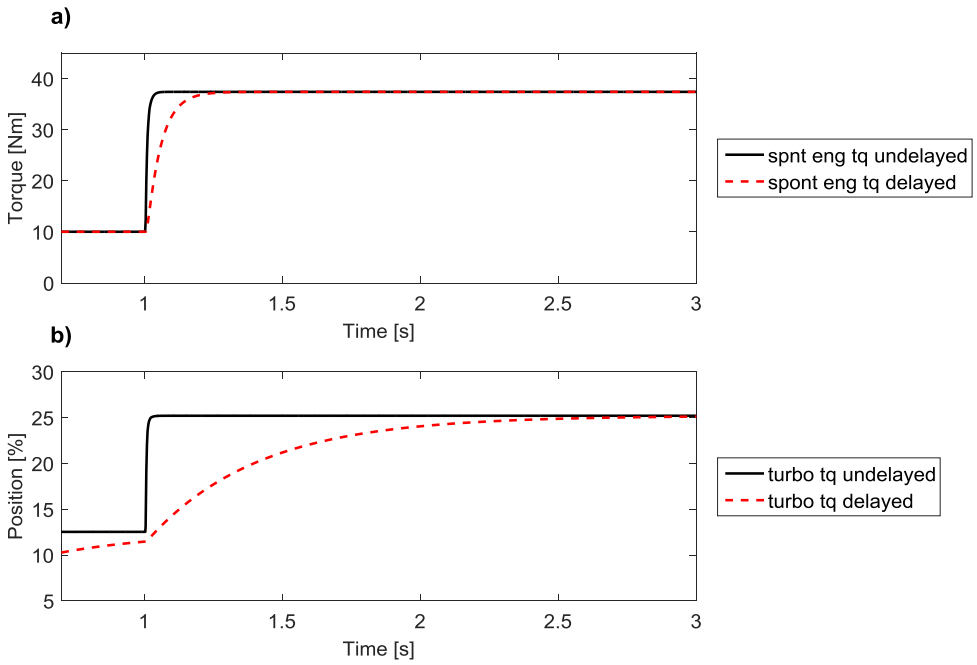

Figure 25: a) Spontanious engine torque delay comparison, b) Additional turbo torque delay comparison

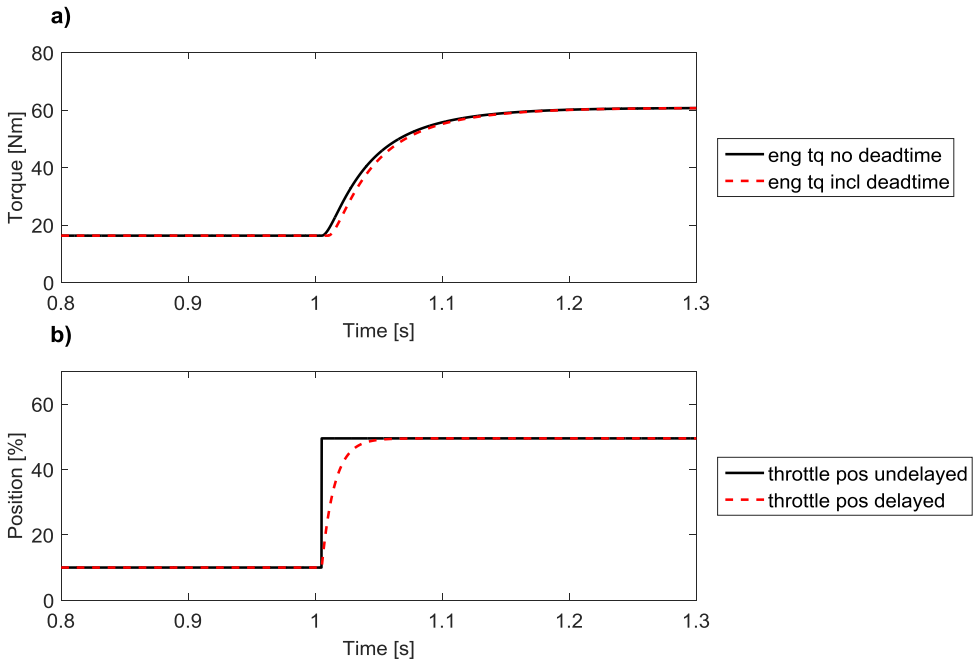

Figure 26: a) Comparison of speed dependent engine torque deadtime, b) Throttle barrel delay comparison

5.2.2 Turbocharger

A thermodynamic model would need extra calculation of engine intake mass flow, temperatures and turbocharger data itself. Neither the turbocharger data was available nor does the modelled engine provide the needed substance states for a thermodynamic model. Blundell and Harty (2004) propose to use differential equations to model the delayed torque build-up of a turbocharger. For the application in this thesis solution seems to fit well, it requires less computation resources than the thermodynamic model and no additional substance state calculations. With two torque maps, one for the engine in naturally aspirated mode and one for the additional turbo torque, the total engine torque output is simulated. To depict the turbo torque build-up a PT1 element

$$T_{tc}\,\dot{M}_{tc,del} + M_{tc,del} = M_{tc} \tag{53}$$

is used. Where T_{tc} is the time constant for the PT1, M_{tc} is the theoretically available turbocharger torque from the turbocharger torque map and $M_{tc,del}$ is the delayed turbocharger torque output. **Figure 27** shows boost pressure build-up times for an inline 4 cylinder turbocharged engine. The size of the engine, turbocharger and the cylinder number is different from the 6 cylinder engine modelled in this thesis, but a general assumption about the delay behaviour can be made.

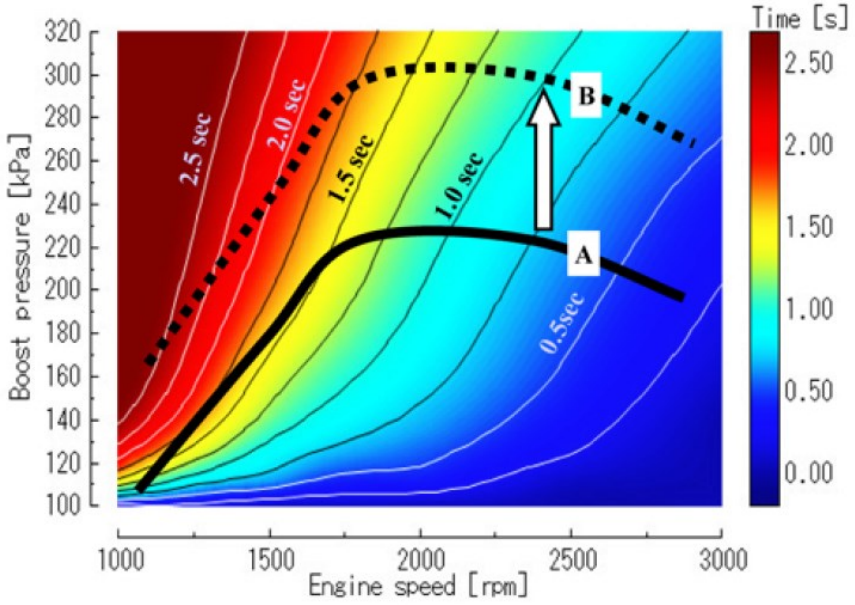

Figure 27: Turbo boost pressure build-up time for an inline 4 cylinder turbocharged engine (Park, Matsumoto, and Oda 2010, p.3)

What can be seen in **Figure 27** is that the time to reach the same boost pressure is smaller at higher engine speeds. This means that modifying the time constant of the PT1 element with engine speed and load can improve the correlation with the real engine. The solution of lowering the time constant at higher engine speeds is depicted in the work of Blundell and Harty (2004). To estimate the time constant for the delay parametrisation, the boost pressure or torque build-up times from Park, Matsumoto, and Oda (2010), Basshuysen (2013), Yamashita, Ibaraki, Sumida, Ebisu, An, and Ogita (2010) and Nishiwaki, Iezawa, Hideyuki Tanaka, and Goto (2013) are analysed. All engines perform a torque step from low torque to full load at low engine speed and are gasoline engines. The time the engines take to reach the demand torque, starting from the torque demand step, varies from *1,5s* to *2,1s*. **Figure 28** shows the torque delay for two engines after a torque step from *20Nm* to full load at an engine speed of *2000 n/min*. Both engines need approximately *2s* to reach the demand torque. Using the information from several sources and taking into account that the turbocharger is designed bigger, due to its electrical support, the time constant T_{tc} was parametrised with *0,4s* and results in a torque delay of approximately *3s* without the help of the electric motor.

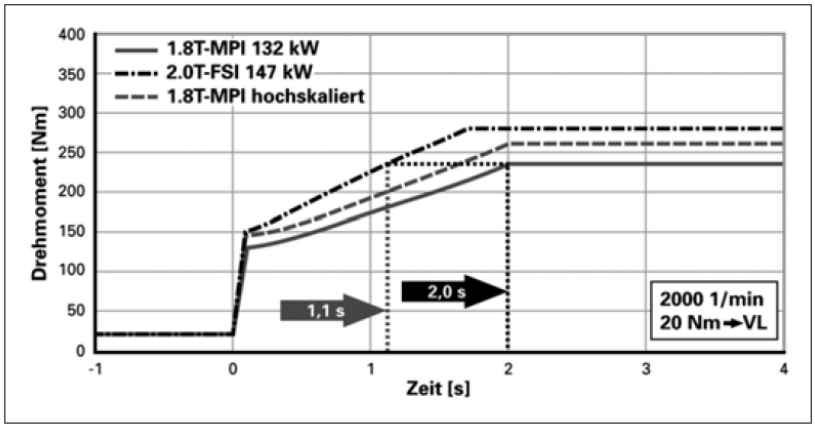

Figure 28: Torque delay after a torque demand step from low load to full load for two different engines (Basshuysen 2013, p.156)

This model approach opens up possibilities for additional implementations. When a fast torque step down in engine torque is needed, a wastegate is opened. A wastegate is a valve, that opens a bypass for the exhaust gas around the turbine. As mentioned before the turbocharger depends strongly on the exhaust gas mass flow. When the turbocharger is operating providing boost pressure, the compressor performs work, driven by the turbine. When the wastegate opens, the turbine can no longer provide the work needed for the compression and the boost pressure starts to drop. Due to the turbochargers inertia and the flow characteristics through the wastegate this is not instantaneous. But compared to the exhaust gas mass flow build-up with engine speed and load, this exhaust gas mass flow reduction is quicker. Therefore the time constant T_{tc} for the turbocharger torque delay needs to be smaller than the before mentioned value of *0,45s* when the wastegate is opened. Using the same approach an electric motor connected to the turbocharger is implemented. The turbocharger delay results from the not present exhaust gas mass flow at lower engine speeds and the turbocharger inertia. **Figure 29** shows a comparison between a conventional two stage turbocharger and an electrically assisted two stage turbocharger. It is visible how the electrically assisted system results in smaller torque delay. Allthough the electrical assisted compressor is a supercharger, the idea of

reducing the turbo lag by electrical support and thereby applying additional power to accelerate the compressor or a whole turbocharger is the same.

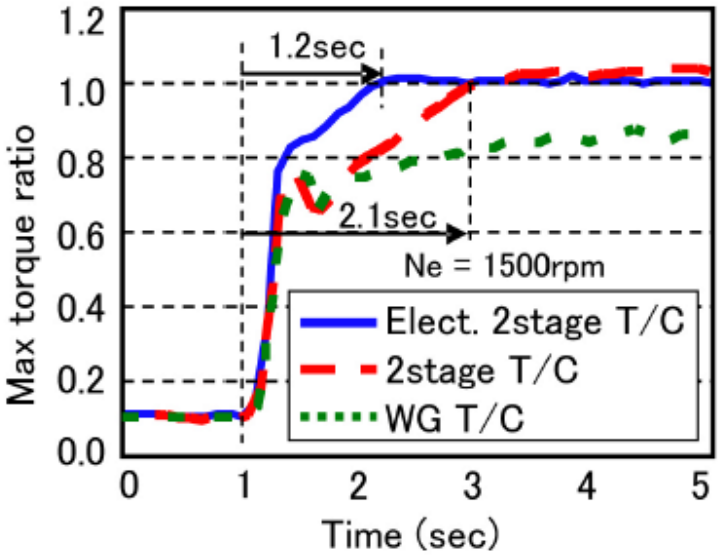

Figure 29: Comparison of step response of a conventional two stage turbocharger and an electrically assisted two stage turbocharger (Nishiwaki, Iezawa, Hideyuki Tanaka, and Goto 2013, p.4)

In the case of this thesis an electric motor helps the turbocharger to accelerate faster and therefore the torque delay becomes smaller. No additional electric motor is modelled but only the delay constant T_{tc} is changed dependent on the desired amount of electric support. **Figure 30** shows the turbocharger torque build up with and without the help of the electric motor. This installation allows for higher turbo dynamics, in acceleration as well as in deceleration. In reality the electric motor can not only feed kinetic energy into the system, but also extract some by converting it into electric energy. As mentioned before no electric motor is modelled and thereby when electric support is demanded additionally to an open wastegate in the model, the lowest possible time constant is used.

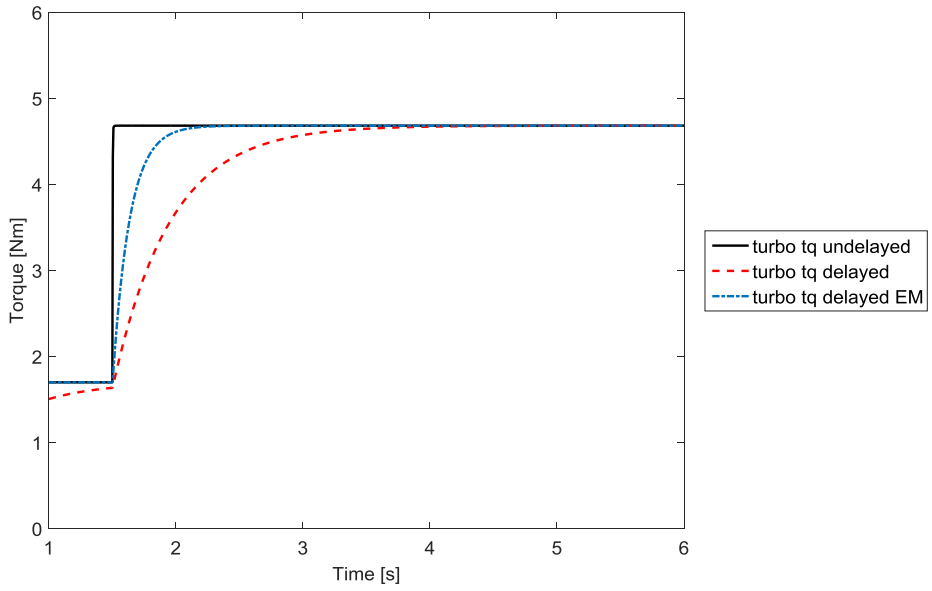

Figure 30: Turbocharger dynamics electric motor assisted

5.2.3 Electric motor

The Powerunit has an additional electric motor, which is connected to the crankshaft through fixed gears. Its output torque is given by a lookup table in relation to speed and a percentage of its possible maximum output. **Figure 31** shows the maximum torque and power curves for the electric motor. The electric motor is connected through idler gears to the crankshaft, therefore the table is already filled with transformed figures for torque at the crankshaft. This additional momentum source is then added to the engines output torque. To replicate the influence of the electric motors mass, its rotational inertia is transformed to the crankshaft as well and added to the engines inertia.

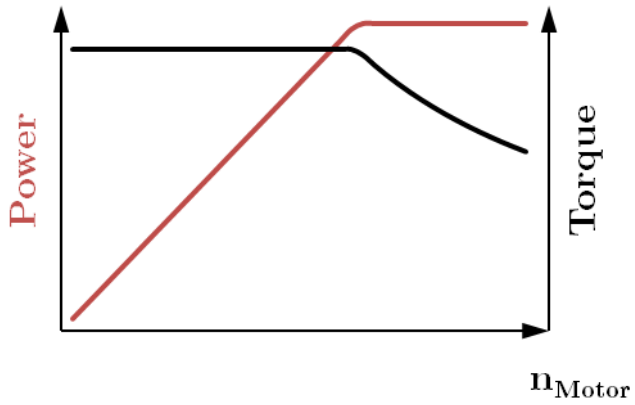

Figure 31: Torque and power curve electric motor

5.3 Engine control unit

The engine control unit (ECU) is responsible for engine control and communication. This block processes all inputs, like driver demand, setpoints or torque interventions signals coming from the transmission control unit. These intervention signals are then converted to signals for the actors on the engine to control its speed and torque output. Because the signals are transmitted via a bus system there is a maximum refresh rate. In a high transient operation mode these are not negligible delays and can be implemented by a constant time delay block. The ECU has an idle controller implemented that is based on a PID controller. The idle controller uses the difference between the actual speed and the target idle speed to control the throttle valve. Furthermore the ECU sends out the demand values for the electric motors on the crankshaft and turbocharger.

5.4 Clutch

The powertrain uses a multiplate dry clutch. This design allows keeping the diameter of the clutch small and by that the rotational inertia is much lower compared to a single plate clutch with the same transmittable torque. An axial force presses the friction plates together. Between each friction plate pair, dependent on their relative rotational speed difference, friction torque originates. The respective plates can slide in axial direction on plate guides which hold the

clutch plates in place. Due to the torque build up, a normal force originates acting on the plate guides to counteract the rotation of the clutch plates. This normal force causes again a friction force alongside the guides. Dependent on the actual torque the clutch is transferring, this friction force acts against the axial movement and therefore reduces the amount of axial force the plates are seeing. This means, that starting from the first plate there is an axial force loss from plate to plate up to the last one (Gradowhl, Belšak, & Hirz 2017, p.4). This uneven force distribution causes different friction torques between the plate pairs and is an important phenomenon in multiplate clutches that needs to be modelled for correct clutch behaviour.

5.4.1 Axial clutch model

This section describes an axial multi body system which represents the axial behaviour of the clutch. This is used to obtain the actual acting clamp force between each plate pair.

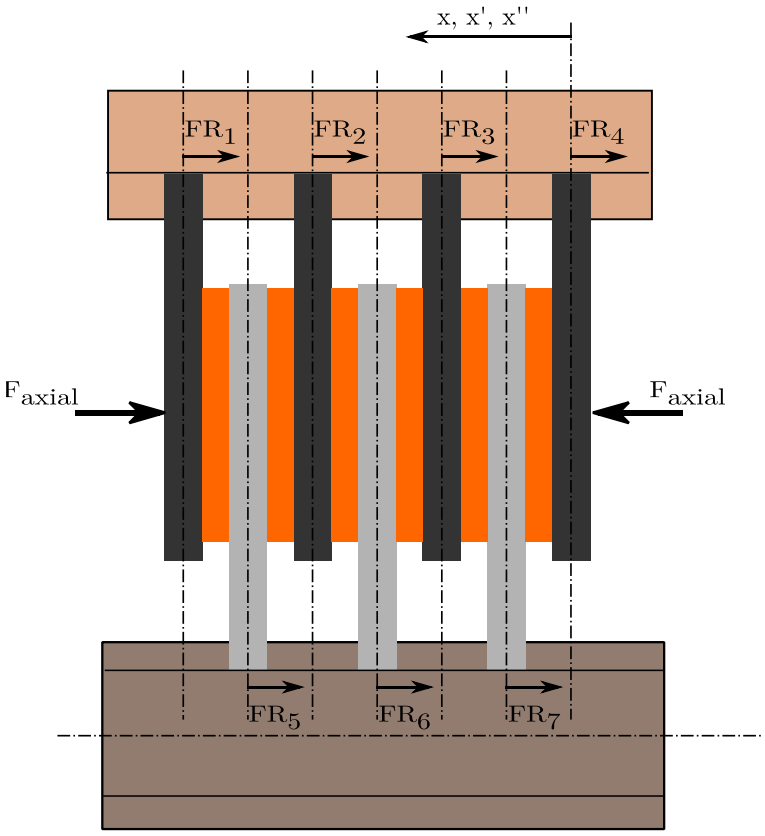

Figure 32: Schematic of the multiplate clutch

The friction forces between one plate and its guides can be assumed in the middle of the plate (Gradowhl, Belšak, & Hirz 2017, p.7). As a consequence of that, between each friction force is half a friction plate, an entire friction pad and half of the friction pad carrier plate. For these three elements a substitutional stiffness $c_{onepack}$ and damping rate $d_{onepack}$

$$c_{onepack} = \frac{1}{\frac{\frac{t_{fplate}}{2}}{E_{fplate}\,A_{fplate}} + \frac{t_{fpad}}{E_{fpad}\,A_{fpad}} + \frac{\frac{t_{fpcplate}}{2}}{E_{fpcplate}\,A_{fpcplate}}} \tag{54}$$

$$d_{onepack} = \frac{1}{\frac{2}{d_{fplate}} + \frac{1}{d_{fpad}} + \frac{2}{d_{fpcplate}}} \tag{55}$$

can be defined (Gradowhl, Belšak, & Hirz 2017, p.7). With E_{fplate} defining the young modulus of the friction plate material and A_{fplate} describing the friction surface.

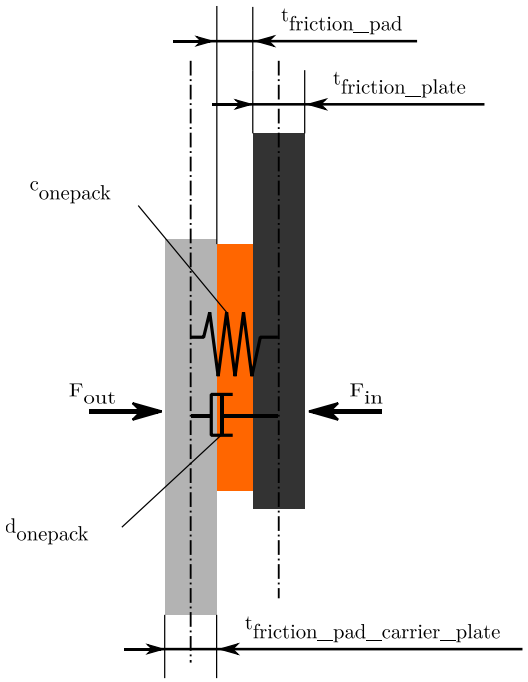

Figure 33: Clutch plate pair detail with substitutional stiffness and damping rate

Using the substitutional stiffness and damping rate the plates are connected to each other and form a multibody system. For each plate the equation of motion

$$m_{fplate}\,\ddot{x}_{fplate} = F_{in} - F_{out} - F_R \tag{56}$$

$$F_{in} = \left(x_{fplate,i} - x_{fpcplate,i}\right) c_{onepack} + \left(\dot{x}_{fplate,i} - \dot{x}_{fpcplate,i}\right) d_{onepack} \tag{57}$$

$$F_{out} = \left(x_{fpcplate,i} - x_{fplate,i+1}\right) c_{onepack} + \left(\dot{x}_{fpcplate,i} - \dot{x}_{fplate,i+1}\right) d_{onepack} \tag{58}$$

can be defined. For the first and last plate the substitutional stiffness and damping rate need to be for half of the thickness of the plate, and the present forces which act over the system boundaries. To model the friction force the LuGre friction model is used. The plates are very light in comparison to the acting forces and due to the multibody system there are oscillations which cause many stick-slip effects. The LuGre model can depict preslide and stick-slip effects and also other friction phenomena very well and was therefore chosen (Olsson 1996, p.51). The difficulty with this model are the parameters that define the friction behaviour. Because the model is built on virtual bristles, the properties in damping and stiffness need to be matched to each system. To this point the clutch is in development and no measurements can be provided to validate. Also because this is not a common approach to model a multiplate clutch, no data of existing clutches could be found which shows the displacement, speed and acceleration of each plate in relation to the transmitted torque. To overcome this problem a solution in general friction description and behaviour had to be found. Olsson (1996) describes in his work how realistic friction behaviour looks like. With experiments he shows wrong behaviour of the model (Olsson 1996, p.59-73). Based on that, it was possible to achieve realistic stick-slip effects and tune the parameters so that not possible behaviour is avoided. It has to be noted, that the clutch is a dry clutch, therefore the before mentioned viscous friction F_V is not taken into account. Summing up the axial forces acting on the friction pads, results in the total residual clamp force. This residual clamp force is then multiplied by dynamic and static friction coefficients to obtain the maximum transmittable torque. The friction coefficient is dependent on heat, clamp force and differential speed of the surfaces. Speed dependant change in friction is

described in the rotational model. Clamp force and heat influence on the coefficient can be depicted by a look up table and a heat generation model. As mentioned before the normal force on the guides depends on the transmitted clutch torque which therefore has to be led back to the axial model from the rotational model. The total transmitted torque has then to be split up into the respective torques acting between the plate pairs. This is done by calculating the percentage of the total clamp force that acts on each plate pair. Because the friction coefficients are assumed static, it is possible to multiply the transmitted clutch torque with the percentages calculated from the clamp force to obtain the respective torques between each plate pair. If a dynamic friction coefficient that depends on heat or clamp force would be needed, then additional to the percentage calculation an inverse look up table of the dependencies has to be implemented to get the actual acting torque between each plate pair. An exemplary clutch closing is depicted in **Figure 34**. Immediately noticeable are the high frequency oscillations at breaking loose seen in the acceleration of the plate $\ddot{x}_1$. These oscillations are induced by the stiffness and the low weight of the clutch plates. **Figure 34b)** and **d)** show the effect of normal force FN that depends on the actual transmitted clutch torque, on the acceleration of the plate.

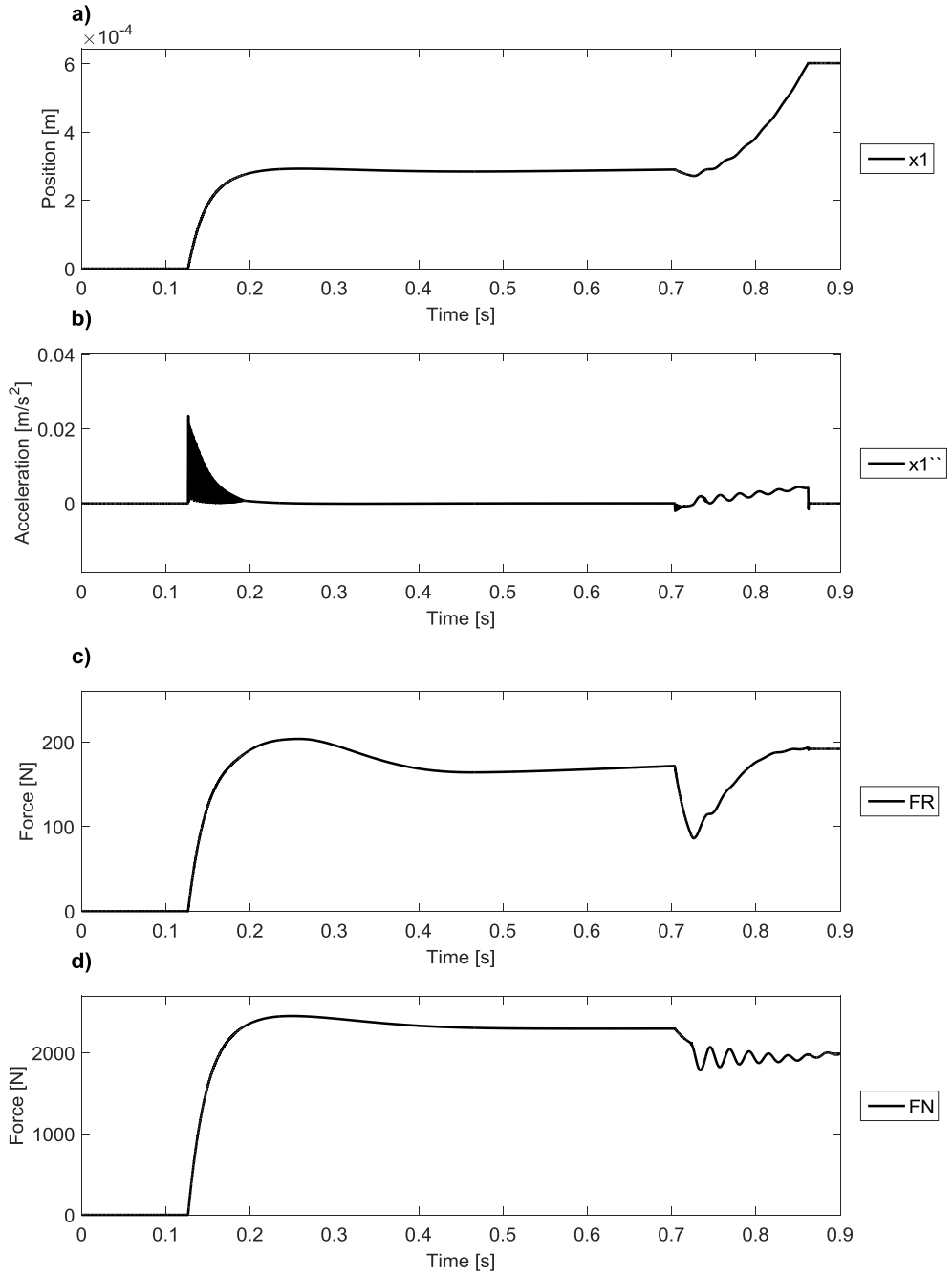

Figure 34: Axial displacement x_1, speed and acceleration $\ddot{x}_1$ of one clutch plate in relation to Normal force FN on the plate guides and resulting FR acting against the clutch plates axial movement

Due to the friction, a hysteresis in the plate movement versus the acting axial force can be seen. **Figure 35** shows a closing, opening and another closing of the clutch from its bitepoint to fully closed position.

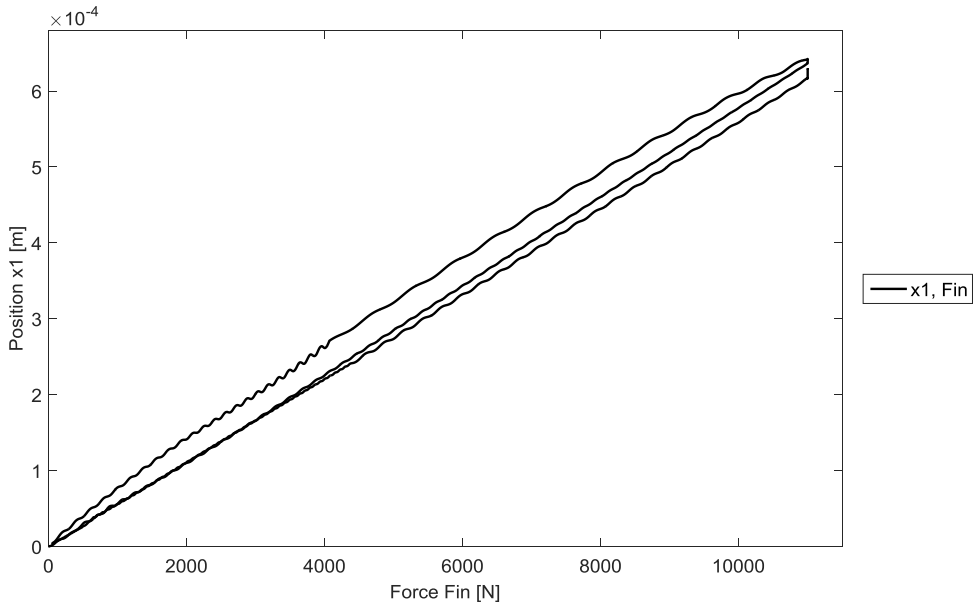

Figure 35: hysteresis of one clutch plate in movement x_1 versus axial force Fin

5.4.2 Rotational model

The rotational model of the clutch is build up using two inertias, one for the primary side and one for the secondary side. Stiffness and the dampening rates of the shafts that connect the primary side to the engine and the secondary side to the transmission, are modelled in the couplings between each model. One of the requirements for this model was the ability to run in realtime. Therefore, the rotational clutch model can be used for Hardware in the loop (HIL) tests in the future. This fact rules out the more complex friction models, like the bristle models. It was desired to have matching speeds in the stick phase and therefore the models with steep static friction curves, like the tanh approximation were dismissed. The most suitable friction model for the requirements is the Karnopp model. With the delta speed area it fulfills the demand for zero speed difference output including correct torque figures. The Karnopp model is still a very simple friction model which is able to run in realtime. As mentioned in the axial model description, the total residual clamp force is multiplied with static and dynamic

friction coefficients to calculate the maximum transmittable torques. These torques serve as input for the dynamic and static torque limitations the Karnopp model is using.

5.5 Transmission

The transmission is modelled by the company in LMS Amesim and planned to perform the investigations upon in the future. A full hydraulic system with line lengths, valves, oil characteristics is included. Synchronizer models are parametrized with their mass, cone shape and friction characteristics, so that the time needed for synchronization matches the predictions of the manufacturer. Besides a shift fork friction, also a detent force is applicable. Gear models are defined by their amount of teeth and inertia. The Transmission requires current inputs which control the hydraulic valves. The valves then control the hydraulic pressure, thereby inducing a movement of the shift actuators.

5.6 Transmission control unit

The TCU calculates and sends out all signals and currents to the clutch and transmission. It also communicates with the ECU for torque intervention requests. For now the currents the TCU sends out are configured manually. The Clutch is controlled through a simple PID for clutch in procedure, and the rest is manually predefined. The clutch signal is a position demand in percent of the maximum travel at full clamp force. This demand is then transformed into the acting clamp force on the first clutch plate. For controller development in the future an actuator model similar to those in the transmission would be beneficial.

5.7 Driveshafts

The driveshafts are modelled within the transmission model with rotary stiffness and damping rate coefficients.

5.8 Couplings

The separate models are coupled by using rotary stiffness and damping rate elements. This type of coupling can be used to model not only stiff connections, but also shafts, which is ideal for this application as all the components in reality are also coupled through shafts. The coupling uses the input and output speeds from the attached submodels as input signals. With the differential speed and angle calculated the transferred torque can be established. This torque is then sent as an input to the following adjacent submodel and also as a feedback torque to the previous submodel.

6 Simulation and results

After all submodels were created and coupled together simulations for power on up shifts could be carried out. **Figure 36** shows an exemplary shift from 1st to 2nd gear. In this shift a more or less conventional, but still sporty approach is shown. The car is already in motion with a fully closed clutch and the driver steps on the accelerator pedal to bring the engine in full load. The car accelerates and when the engine reaches the desired revolutions a shift is performed. Therefore the clutch demand is set to zero and shortly after that the throttle demand is reduced. Due to reaction time and delays the torque of the clutch and engine almost simultaneously begin to drop. Additionally to closing the throttle, ignition retardation takes place. The engine torque reacts almost instantly to this intervention. To lower the negative engine speed gradient even more, the electric motor on the crankshaft outputs a negative torque. Parallel to that, as soon as the clutch torque is close to zero, the torque through the synchronizer and thereby the force preventing the synchronizer sleeve to move is also small enough to disengage the gear. After the synchronizer sleeve reaches its neutral position the sleeve of the gear to engage can start to move towards the synchronizer friction cone to build up axial force and start to decelerate the shaft. The shaft is mechanically connected to the secondary side of the clutch and so the synchronization process can be seen by the deceleration of the secondary clutch revolutions in **Figure 36a**). This process is also visible looking at the shiftfork positions graph depicted in **Figure 36d).** Shiftfork C starts to move from its neutral position in the negative direction. There it stops on its way because the synchronizer body has a different speed than the gear and the friction torque caused by the synchronizer cone results in a counteracting axial force due to its geometry. As soon as the speeds are synchronized this counteracting axial force disappears and the sleeve can move to its final position and lock the synchronizer geometrically. This new gear ratio defines the speed of the secondary clutch side and thereby the speed the engine should ideally have to close the clutch to not have torque pikes in the drivetrain. Knowing the engine speed to reach, the assistance of the electric motor is reduced and finally completely stopped. It is

also visible that the throttle is opened before the ignition retardation is removed. That is due to the delays described earlier.

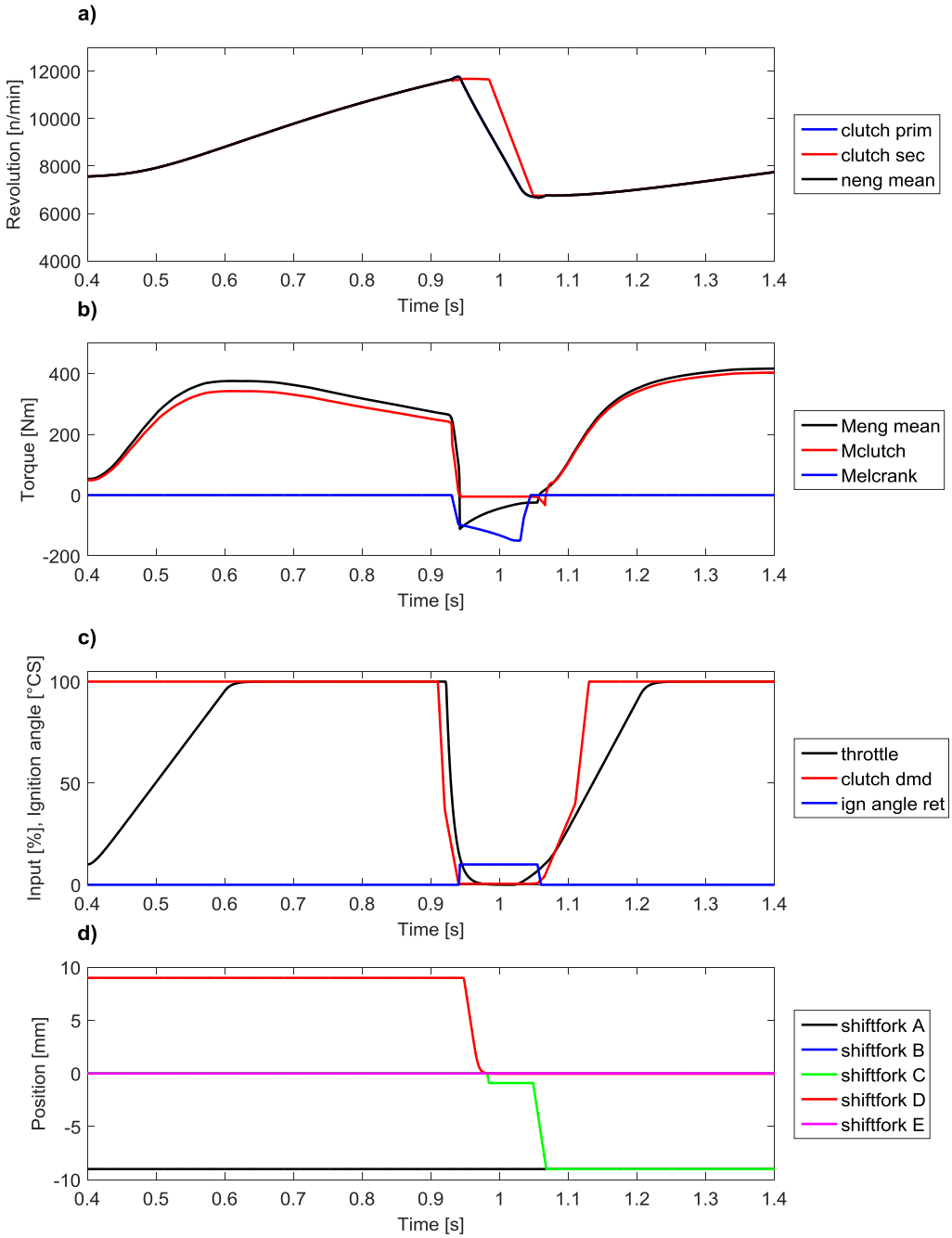

Figure 36: Shift from 1st to 2nd, full throttle with clutch and electric motor assistance on turbocharger and crank, a) relevant speeds of engine, primary and secondary side of the clutch, b) torques of the engine, clutch and the electric motor connected to the crankshaft, c) input demands for throttle, clutch and ignition angle retardation, d) position of the shiftforks

As soon as the synchronization is complete and the engine has the correct speed, the ignition retardation is reduced to zero and the clutch is closed. The throttle pedal is brought back up to full load and the car continues to accelerate. What can be seen in **Figure 37a)** is the torque limitation of the electric motor following a hyperbola when it reaches its maximum power. Looking at the engine torque in the deceleration phase, the quadratic curve of the friction torque is visible in **Figure 37b)**. Looking at the clutch torque curve showed in **Figure 36b),** a small negative pike can be seen. This is because the engine speed is not absolutely correct, but a small amount faster than the secondary clutch side. The pike originates from the deceleration of the engines inertia to the secondary clutch speed.

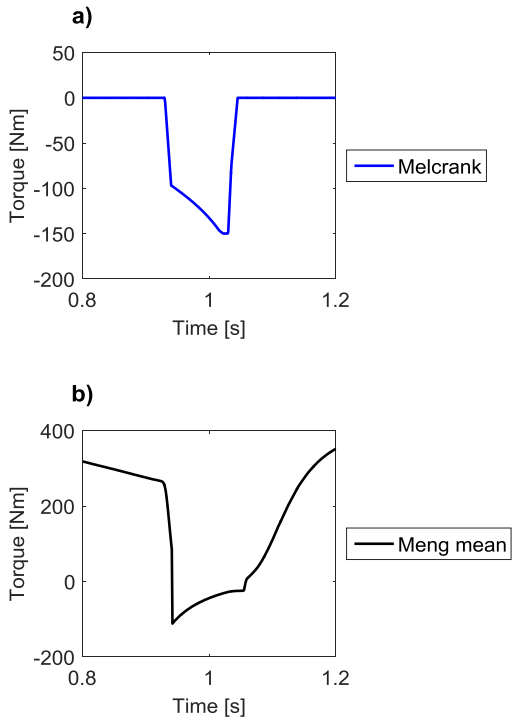

Figure 37: a) Detail of electric motor torque curve, b) detail of engine torque with visible friction amount

A more radical approach for the entire shift would be to open the clutch only for the synchronizer engagement as shown in **Figure 38**. This means in the first step engine torque is reduced by ignition retardation while the throttle stays wide open. The pressure on the synchronizer to disengage the gear is ramping up to a

safe amount without damaging the components. When the torque of the engine is around zero or small enough to overcome the locking of the synchronizer, the sleeve can move out of the lock and go into its idle position, thereby disconnecting the gearbox shafts. Using the still connected engine and electric motor, the clutch and inputshaft can be decelerated to the speed the next gear would require. Close to a defined delta speed of the inputshaft to the spinning gear, the clutch can open fully or only partially to smoothen the engagement of the synchronizer for the next gear. This shifting method should bring fast shift times because the synchronization is accelerated by engine and the electric motor on the crankshaft and not done solely by the synchronizer itself. Only for the last part of the shift the clutch and synchronizer are needed to eliminate any residual differential speeds. Comparing the two shifts it is visible that the engine and clutch torque are much faster recovering from the shift interruption. The throttle stays open all the time while the intervention is done only by ignition retardation and the electric motor on the crankshaft. Due to this fact the gradient of the positive torque after the shift is quite steep. Looking at the engine speed and secondary clutch speed a difference is visible when the torque is back up again. The clutch slipping reduces the torque impact.

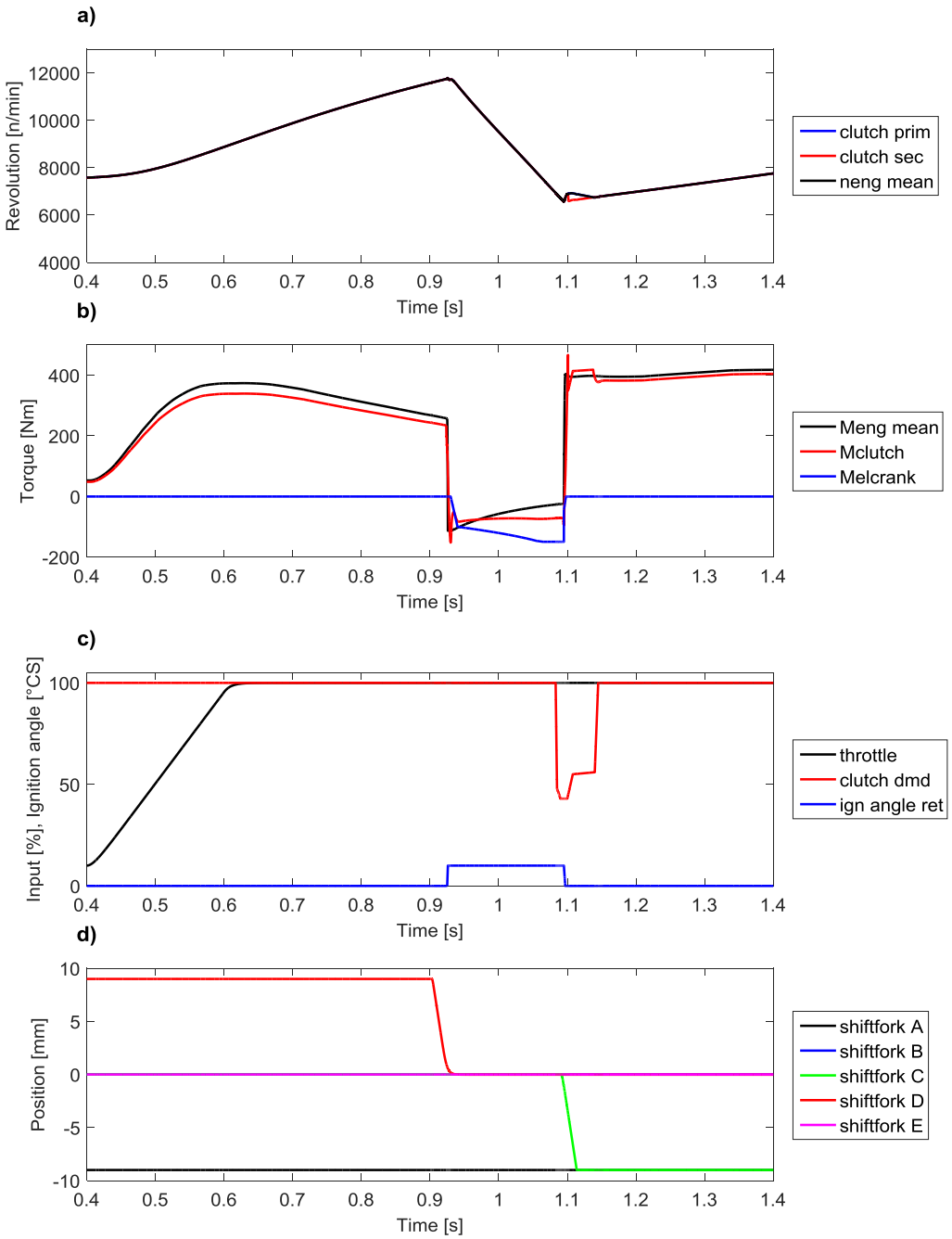

Figure 38: Partial clutch shift 1st to 2nd, a) relevant speeds of engine, primary and secondary side of the clutch, b) torques of the engine, clutch and the electric motor connected to the crankshaft, c) input demands for throttle, clutch and ignition angle retardation, d) position of the shiftforks

In comparison to the previous described shift, another shift with less clutch opening was performed to make this dampening effect visible. **Figure 39c) and**

Figure 39g) show the different clutch demand inputs. Looking at the speed graphs, one can notice the clutch slip in **Figure 39e)**, while there is none present in **Figure 39a)**. This means the clutch does not open enough to reduce its transmittable torque and the entire impact of the engine torque recovering transfers into the drive train. A high torque peak is the outcome of that and can be seen in **Figure 39b)**. In comparison to that the much smaller torque oscillation in **Figure 39f)**. Slipping effects like this can also be applied in other states of the shift procedure.

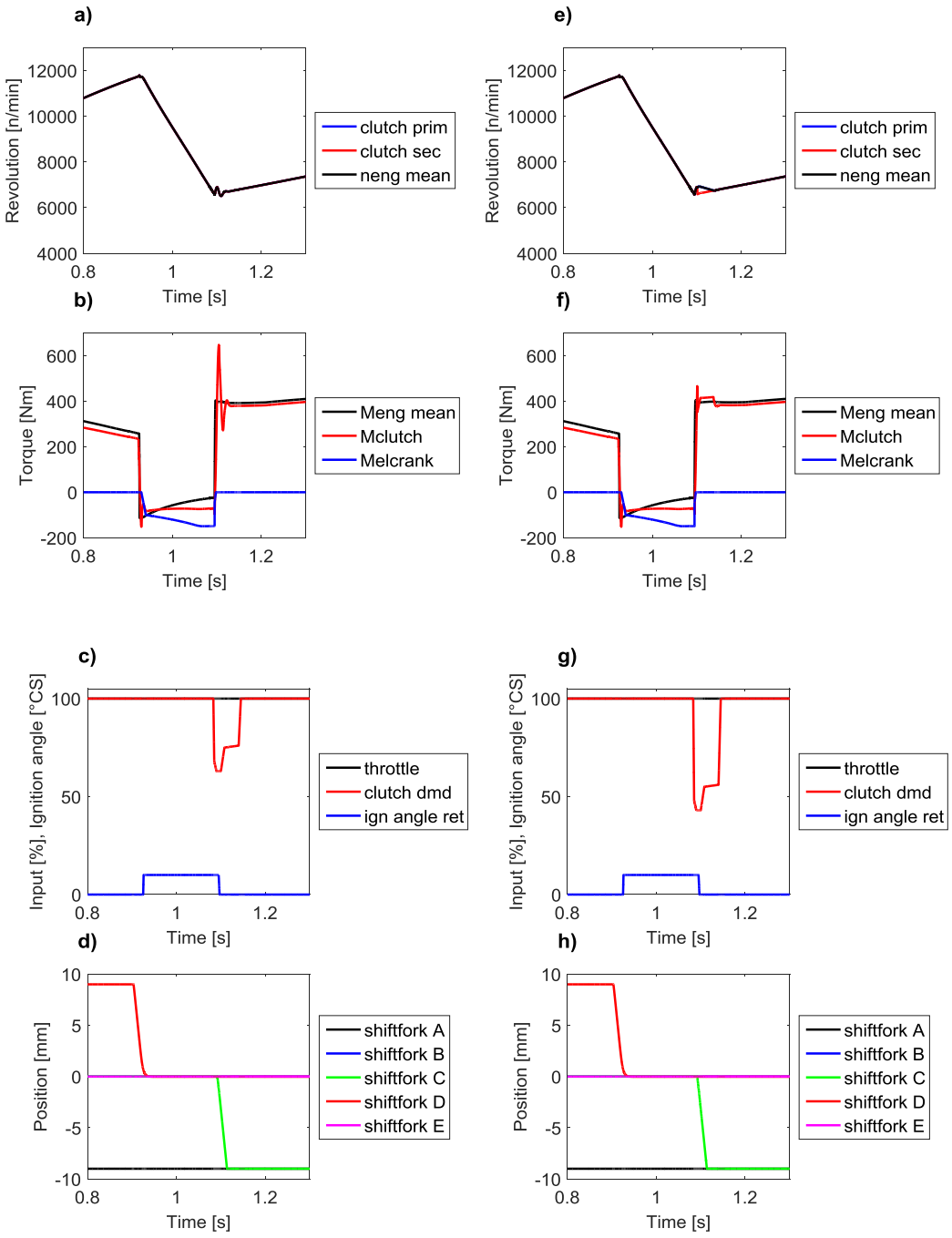

Figure 39: Comparison partial clutch shifts 1st to 2nd, a)e) relevant speeds of engine, primary and secondary side of the clutch, b)f) torques of the engine, clutch and the electric motor connected to the crankshaft, c)g) input demands for throttle, clutch and ignition angle retardation, d)h) position of the shiftforks

7 Analysis and outlook

Different varieties of shift strategies can now be tried out and analysed based on the overall shifttime and the residual differential speed between the primary and secondary clutch sides. This differential speed needs to be eliminated to engage the synchronizer, and the higher the delta speed the more torque is needed to even it out. This torque is spread through the drivetrain and defines how big the jerk felt by the driver will be. One of the possibilities already shown is to keep the throttle open and reduce the torque only by ignition retardation, this will provide a very fast torque recovery but also not as smooth and controllable in comparison to an intervention including throttle and ignition retardation. The reason for this is that ignition angle retardation works only up to a certain point, where the fuel air mixture will still ignite. Moving past this limit the ignition becomes not stable and combustion engine cycle to cycle variations cause alternating ignition. Reaching this point makes the torque no longer controllable. It is possible to define an angle where the ignition is completely cut out and avoid the alternating ignition. To help controlling the powerunit output torque the electric motor on the crankshaft can play an important role. A smoother transition from the lowered torque to the ignition cut and from the cut to positive torque can be implemented.

8 Conclusion

In this thesis the creation of the simplified longitudinal model for the simulation of high dynamic shifts on an automated manual transmission was explained. The origins of the demanded engine oscillations were analysed and modelled. An insight into the buildup of the components and the modelling solutions therefore were presented. A solution for the multiplate clutch with axial force loss was found, described and applied. Three upshifts were presented and analysed to show the entire systems behaviour and to explain which investigations can be performed in the future using this model. For accurate results correlation of the single components needs to be done when the real parts and data from measurements are available. At this stage general shift investigations can be performed to show how a shift process can look like and test different shift procedures. Even if not all parameters are correlated yet, consequences like torque pikes or induced oscillations reveal areas where problems can occur with the real components and need to be concentrated on.

References

Basshuysen, R., (2013). *Ottomotor mit Direkteinspritzung: Verfahren · Systeme · Entwicklung · Potenzial* (3rd edn.) BadWimpfen. Springer Vieweg. ISBN 978-3-658-01407-0

Bataus, M., Maciac, A., Oprean, M., Vasiliu, N., (2011). *Automotive Clutch Models for Real Time Simulation.* University "Politehnica" of Bucharest, Bucharest. The publishing house proceedings of the Romanian academy, Series A, Volume 12, Number 2/2011, (pp. 109–116).

Blundell, M. and Harty D., (2004). *Multibody Systems Approach to Vehicle Dynamics.* Elsevier Butterworth-Heinmann. ISBN 0 7506 5115 1

Caton, A. J., (2016). *An Introduction to Thermodynamic Cycle Simulations for Internal Combustion Engines.* Texas A&M University, College Station, TX. John Wiley & Sons Ltd. ISBN: 9781119037569

Chen, J.-S., (2008). *Mean Value Engine Model Using Object Oriented Modeling.* Paper for Conference SAE World Congress & Exhibition 14.04.2008, MI, Detroit. DOI: 10.4271/2008-01-0982

Gradowhl, C., Belšak, A., & Hirz, M., (2017). *Dynamic simulation of multi-plate clutches for automotive applications.* Graz University of Technology, Graz. University of Maribor, Maribor. Paper for Science and Motor Vehicles Conference 19.03.2017, Belgrade.

Guzzella, L. and Onder, C. H., (2004). *Introduction to Modeling and Control of Internal Combustion Engine Systems.* ETH Zurich, Zurich. Springer-Verlag Berlin Heidelberg New York. ISBN 978-3-642-06085-4

Hendricks, E., & Sorenson, S. C. (1990). Mean Value SI Engine Model for Control Studies. Technical University of Demark, Denmark. Published at American Control Conference 29.06.-01.07.1990 (pp. 1882-1887). IEEE.

Isermann, R., (2014). *Engine Modeling and Control: Modeling and Electronic Management of Internal Combustion Engines.* Technical University Darmstadt, Darmstadt. Springer-Verlag Berlin Heidelberg. ISBN 978-3-642-39933-6

Lechner, G., & Naunheimer, H., (1999). *Automotive Transmissions.* Berlin, Heidelberg, New York, Barcelona, Hong Kong, London, Milan, Paris, Singapore, Tokyo. Springer-Verlag Berlin Heidenberg New York. ISBN 3-540-65903-X

Matthies, F., (2013). *Beitrag zur Modellbildung von Antriebsträngen für Fahrbarkeitsuntersuchungen.* Berlin Technical University, Berlin. epubli GmbH, Berlin. ISBN 978-3-8442-6704-4

Merker, G. P., Schwarz, C., and Teichmann, R., (2009). *Combustion Engines Development: Mixture Formation, Combustion, Emissions and Simulation.* Tettnang, Munich, Graz. Vieweg & Teubner. ISBN 978-3-642-02951-6

Nishiwaki, K., Iezawa, M., Hideyuki Tanaka, H., and Goto, T. (2013). *Development of High Speed Motor and Inverter for Electric Supercharger.* SAE International. DOI 10.4271/2013-01-0931

Olsson, H., (1996). *Control Systems with Friction.* Department of Automatic Control Lund Institute of Technology, Lund. ISSN 0280–5316

Park, S., Matsumoto, T., and Oda, N., (2010). *Numerical Analysis of Turbocharger Response Delay Mechanism.* Shimotakanezawa. SAE International. DOI 10.4271/2010-01-1226

Pischinger, R., Klell, M., Sams T., (2009), *Thermodynamik der Verbrennungskraftmaschine* (3rd edn.). Graz University of Technology, AVL List GmbH, Graz. Springer-Verlag Wien New York. ISBN 978-3211-99276-0

Roddeck, W., (2003). *Einführung in die Mechatronik* (2nd edn.). Bochum University of Applied Sciences, Bochum. Springer Fachmedien Wiesbaden. ISBN 978-3-322-91180-3

Schreiner, K., (2015). *Basiswissen Verbrennungsmotor: Fragen - rechnen - verstehen – bestehen* (2nd edn.). HWTG Konstanz University of Applied Sciencees, Konstanz. Springer Vieweg. ISBN 978-3-658-06186-9

Siemens Product Lifecycle Management Software Inc.. *LMS Amesim.* https://www.plm.automation.siemens.com/global/en/

Sinsel, S., (2000). *Echtzeitsimulation von Nutzfahrzeug-Dieselmotoren mit Turbolader zur Entwicklung von Motormanagementsystemen.* (Doctoral dissertation) Technical University Darmstadt, Darmstadt. Logos Verlag Berlin. ISBN 978-3897223561

The Mathworks, Inc. (2015). *MATLAB Simulink.* Product version 8.6.0.259410. Released at 21:10, 30.07.2015. https://ch.mathworks.com/?s_tid=gn_logo

Theotokatos, G. P., (2009) *A Comparative Study on Mean Value Modelling of Two-Stroke Marine Diesel Engine.* School of Technological Applications TEI of Athens, Egaleo. Paper for WSEAS International Conference on Maritime and Naval Science and Engineering 24-26.09.2009, Brasow. ISBN: 978-960-474-120-5

Urlaub, A., (1989a). *Verbrennungsmotoren: Band 1, Grundlagen.* Berlin, Heidelberg, New York, London, Paris, Tokyo, Hong Kong. Springer-Verlag Berlin Heidelberg. ISBN: 978-3-540-51230-1

Urlaub, A., (1989b). *Verbrennungsmotoren: Band 3, Konstruktion.* Berlin, Heidelberg, New York, London, Paris, Tokyo, Hong Kong. Springer-Verlag Berlin Heidelberg. ISBN: 978-3-540-51230-1

Yamashita, Y., Ibaraki, S., Sumida, K., Ebisu, M., An, B., Ogita, H. (2010). *Development of Electric Supercharger to Facilitate the Downsizing of Automobile Engines.* Published in Mitsubishi Heavy Industries Technical Review Vol. 47 No. 4, 12.2010

Chaing W.-P., Zhu, L., and Patankar, R. (2007). *Mean Value Engine Modeling and Validation for a 4-stroke, Single Cylinder Gasoline Engine.* Michigan Technological University, Houghton, MI. Academic Journals. Published in Trends in Applied Sciences Research 2 (2): 124-131. ISSN 1819-3579

List of figures